Cell differentiation and matrix organization are differentially affected during bone formation in osteogenesis imperfecta zebrafish models with different genetic defects impacting collagen type I structure

Valentina Daponte, Francesca Tonelli, Cecilia Masiero, Delfien Syx, Chloé Exbrayat-Héritier, Marco Biggiogera, Andy Willaert, Antonio Rossi, Paul J Coucke, Florence Ruggiero, et al.

Cell differentiation and matrix organization are differentially affected during bone formation in osteogenesis imperfecta zebrafish models with different genetic defects impacting collagen type I structure

Valentina Daponte [a], Francesca Tonelli [a], Cecilia Masiero [a], Delfien Syx [b], Chloé Exbrayat-Héritier [c], Marco Biggiogera [d], Andy Willaert [b], Antonio Rossi [a], Paul J. Coucke [b], Florence Ruggiero [c] and Antonella Forlino [a]

***a* - Department of Molecular Medicine,** *Biochemistry Unit, University of Pavia, Pavia, Italy*
***b* - Department of Biomolecular Medicine,** *Center of Medical Genetics, Ghent University and Ghent University Hospital, Ghent, Belgium*
***c* - Institut de Génomique Fonctionnelle de Lyon, Ecole Normale Supérieure de Lyon,** *CNRS UMR5242, UCBL Lyon-1, Lyon F-69007, France*
***d* - Department of Biology and Biotechnology,** *University of Pavia, Pavia, Italy*

Corresponding author at: *Professor of Biochemistry, Department of Molecular Medicine, Biochemistry Unit, University of Pavia, Via Taramelli 3B, 27100 Pavia, Italy.* *aforlino@unipv.it.*
https://doi.org/10.1016/j.matbio.2023.06.003

Abstract

Osteogenesis imperfecta (OI) is a family of rare heritable skeletal disorders associated with dominant mutations in the collagen type I encoding genes and recessive defects in proteins involved in collagen type I synthesis and processing and in osteoblast differentiation and activity. Historically, it was believed that the OI bone phenotype was only caused by abnormal collagen type I fibrils in the extracellular matrix, but more recently it became clear that the altered bone cell homeostasis, due to mutant collagen retention, plays a relevant role in modulating disease severity in most of the OI forms and it is correlated to impaired bone cell differentiation. Despite *in vitro* evidence, *in vivo* data are missing. To better understand the physiopathology of OI, we used two zebrafish models: *Chihuahua* (*Chi*/+), carrying a dominant p.G736D substitution in the α1 chain of collagen type I, and the recessive *p3h1*$^{-/-}$, lacking prolyl 3-hydroxylase (P3h1) enzyme. Both models share the delay of collagen type I folding, resulting in its overmodification and partial intracellular retention. The regeneration of the bony caudal fin of *Chi*/+ and *p3h1*$^{-/-}$ was employed to investigate the impact of abnormal collagen synthesis on bone cell differentiation. Reduced regenerative ability was evident in both models, but it was associated to impaired osteoblast differentiation and osteoblastogenesis/adipogenesis switch only in *Chi*/+. On the contrary, reduced osteoclast number and activity were found in both models during regeneration. The dominant OI model showed a more detrimental effect in the extracellular matrix organization. Interestingly, the chemical chaperone 4-phenylbutyrate (4-PBA), known to reduce cellular stress and increase collagen secretion, improved bone formation only in *p3h1*$^{-/-}$ by favoring caudal fin growth without affecting bone cell markers expression. Taken together, our *in vivo* data proved the negative impact of structurally abnormal collagen type I on bone formation but revealed a gene mutation-specific effect on bone cell differentiation and matrix organization in OI. These, together with the distinct ability to respond to the chaperone treatment, underline the need for precision medicine approaches to properly treat the disease.

Introduction

Osteogenesis imperfecta (OI) is a group of hereditary skeletal disorders sharing reduced bone mineral density, severe bone deformity and frequent fractures [1]. Classical OI refers to the dominantly inherited types I to IV caused by mutations in *COL1A1* and *COL1A2* genes encoding the pro-α1 and pro-α2 chains of collagen type I, respectively [2]. In classical OI the most frequent defects are glycine substitutions within the conserved Gly-Xaa-Yaa triple helix motif. The presence of a bulkier amino acid in place of Gly-results in the delay of the pro-α chains folding that causes their excessive exposure to post-translational modifying enzymes and the intracellular retention of the overmodified molecules [3]. More recently, recessive OI forms have been identified affecting proteins involved in collagen biosynthesis or osteoblasts differentiation and activity [3]. Among these, OI type VIII is caused by biallelic mutations in the enzyme prolyl 3-hydroxylase 1 (P3H1) that belongs to an endoplasmic reticulum (ER) resident complex in which it associates in a 1:1:1 ratio with the chaperone cartilage-associated protein (CRTAP) and the *cis-trans* isomerase cyclophilin B (CyPB). The complex works as a molecular chaperone by favoring triple helix folding, and is responsible for the 3-hydroxylation of a specific Pro986 residue in Xaa-position in the α1(I) chains [4]. 3-hydroxylated Pro986 side chains extend externally from the triple helix axis and favor extracellular assembly of the collagen molecules [5]. Recessive OI type VIII shares with OI classical forms the delay of pro-α(I) chain folding, their overmodification and the intracellular retention of misfolded collagen, leading to cell stress [6,7].

In the last decade it was shown that altered cell homeostasis affects bone cells differentiation. Indeed, an impairment in osteoblast differentiation was described in three OI murine models. The *Brtl* mouse, characterized by a G349C (p.G527C) substitution in α1(I) chain, showed reduced early and late osteoblastogenic markers expression and increased adipogenesis *in vitro* [8]. In the *Amish* mouse, carrying a G610C (p.G777C) substitution in α2(I) chain, reduced transcription of mature osteoblast markers such as *Bglap* was observed both *in vitro* and *in vivo* [9]. Finally, an accumulation of immature osteoblasts and increased osteoclastogenesis was reported in the *Oim* mice, carrying a homozygous nucleotide deletion leading to a frameshift mutation in the sequence encoding the C-terminal propeptide of *Col1a2* [10]. However, detailed information about bone cell differentiation during bone formation in OI patients and mice are still scarce.

Zebrafish (*Danio rerio*) is a proven valid model to investigate skeletal diseases, sharing 71% of homology with human genes and conserving both mammalian bone cells and ossification types [11,12]. Several zebrafish mutants for OI were generated either by forward or reverse genetic approaches, strongly contributing to better dissect the pathology [7,13-15]. Among these, we previously deeply characterized the dominant severe OI type III, *Chihuahua* (*Chi*/+) zebrafish, obtained by ENU mutagenesis and carrying a p.G736D substitution in α1(I) chain [16,17]. More recently, using CRISPR/Cas9 gene editing we generated and characterized the knock-out *p3h1*$^{-/-}$ zebrafish that recapitulates the human OI type VIII phenotype [7].

The advantages in using zebrafish as animal models to investigate skeletal diseases are multiple. First, zebrafish can fully regenerate several organs and tissues, including the bony caudal fin [18]. Fin rays, also called lepidotrichia, belong to the dermal skeleton and are directly formed from osteoblasts without a cartilage template. Each ray is constituted by a repetition of ~20 segments, interconnected by collagenous ligaments called joints. After caudal fin amputation, a regenerative program starts. The first phase is a rapid wound healing followed by the blastema formation, with mature osteoblasts dedifferentiating, becoming proliferative, and migrating distally to form a region of undifferentiated cells (blastema). In the last regenerative outgrowth phase, the bone cells re-differentiate, and the sequentially expression of *runx2* (pre−osteoblast marker), *sp7/osterix* (committed osteoblast marker) and finally *bglap/osteocalcin* (mature osteoblast marker) takes place [19,20]. Osteoclasts are also involved in caudal fin regeneration, indeed after 5−6 days post amputation (dpa) they accumulate at the level of the amputation plane as well as along the regenerating fin rays [21,22]. Zebrafish caudal fin is easily accessible for manipulation, and after amputation it rapidly regenerates within 2 weeks.

Furthermore, being almost fully translucent for quite some time during growth [23], after crossing with transgenic fish lines labeling osteoblasts at different developmental stages, zebrafish provide a unique tool to study bone cell differentiation *in vivo*.

Lastly, thanks to the ability to absorb drugs and compounds from the water through the mouth and the gills, zebrafish provide a convenient tool for drug screening. In particular, the study of caudal fin regeneration after drug administration is nowadays a standardized assay to assess the effect of compounds on bone [24].

Here, caudal fin regeneration allowed *in vivo* investigation of bone formation in the zebrafish *Chihuahua* (*Chi*/+) and *p3h1*$^{-/-}$, models for dominant and recessive OI, respectively, which are both characterized by altered collagen structure.

Results

Caudal fin regeneration is reduced in dominant α1(I) p.G736D (*Chi*/+) and recessive *p3h1*$^{-/-}$

Caudal fin regeneration, a well-known and standardized system to evaluate bone formation in zebrafish, was assessed in WT, *Chi*/+ and *p3h1*$^{-/-}$ OI zebrafish by means of vital calcein staining (Fig. 1A). The regenerated caudal fin area at 7 and 14 days post amputation (dpa) was analysed. To evaluate a possible impact of different developmental stages on regenerative ability, the study was performed in zebrafish at 3 months post fertilization (mpf), representing juvenile to adult transition, and at 8 mpf, corresponding to the adulthood. The regeneration ability was significantly compromised in mutants with respect to WT. The percentage of the Regenerated Area (REG) and of the Estimated Mineralized Area (EMA) were significantly reduced in *Chi*/+ and *p3h1*$^{-/-}$ compared to WT both at 7 and 14 dpa (Fig. 1B-C). No effect of the two tested developmental stages was detectable in the regeneration capacity of WT and mutants. The reduced regenerative ability observed *in vivo* in *Chi*/+ and *p3h1*$^{-/-}$ compared to WT demonstrated an impaired bone formation in both OI models.

The improved bone regeneration following 4-PBA treatment is not affecting bone cell markers expression

Both *Chi*/+ and *p3h1*$^{-/-}$ OI models are characterized by over-glycosylated collagen I, which is retained in the ER [7,17]. The consequent cellular stress therefore represents a possible target for OI therapy.

We previously demonstrated the positive effect of 4-phenylbutyrate (4-PBA) as a chemical chaperone able to improve bone mineralization in *Chi*/+ larvae [17]. Here, we tested 4-PBA effect on adult *Chi*/+ and *p3h1*$^{-/-}$ during caudal fin regeneration to investigate its potential effect on bone formation and gene expression of bone cell-related genes.

The effect of 4-PBA administration on bone regeneration was evaluated on 3 and 8 mpf WT, *Chi*/+ and *p3h1*$^{-/-}$ zebrafish at 7 and 14 dpa by measuring REG and EMA parameters as described above.

4-PBA administration did not show any effect on the regeneration capacity of *Chi*/+ zebrafish at any ages and time points analyzed (Fig. 1B). In 3 mpf at 14 dpa, 4-PBA rescued *p3h1*$^{-/-}$ REG that reached WT value, whereas *p3h1*$^{-/-}$ EMA remained significantly less than untreated WT.

Interestingly, 4-PBA treatment on 8 mpf zebrafish rescued in *p3h1*$^{-/-}$ the delay in bone formation respect to controls at both 7 and 14 dpa. REG and EMA of *p3h1*$^{-/-}$ treated zebrafish reached WT value at 14 dpa. (Fig. 1C).

The effect of 4-PBA treatment on the expression levels of the early (*runx2a, runx2b, sox9a, sox9b*), intermediate (*sp7*) and late (*bglap*) osteoblast markers and on the *acp5a* osteoclast marker were also evaluated on 3 and 5 dpa *Chi*/+ and *p3h1*$^{-/-}$ caudal fins. No difference between WT and mutants at all the analyzed time points was detected for all these genes (Supplementary Figs. 1 and 2).

Taken together, these data indicate that during caudal fin regeneration 4-PBA is not affecting gene expression and its positive chaperone effect is only detectable in the recessive *p3h1*$^{-/-}$ model.

Caudal fin morphology is impaired in dominant *chi*/+ and recessive *p3h1*$^{-/-}$

To deeply investigate caudal fin morphology in adults before and during regeneration, detailed morphometric analysis was carried out in WT, *Chi*/+ and *p3h1*$^{-/-}$ on the original caudal fin (indicated from now on as sample at day 0) and at 7 and 14 dpa. Representative images are shown in Supplementary Fig. 3.

Limited to *p3h1*$^{-/-}$, a significantly reduced number of fin rays in the day 0 caudal fin respect to WT was detectable, suggesting a possible developmental defect in this model (Fig. 2A).

The caudal fin size was significantly reduced only in *Chi*/+ respect to WT (Fig. 2B). While the number of segments did not differ between WT and *Chi*/+ (Fig. 2C), their medium length was reduced at all time points, coherently with the smaller caudal fin that characterizes this mutant (Fig. 2D). On the contrary, an increased number of segments was evident in *p3h1*$^{-/-}$ with respect to WT at day 0 (Fig. 2C), but their length was reduced as in *Chi*/+ (Fig. 2D). At 14 dpa, *p3h1*$^{-/-}$ segment length had normal value, while their number was significantly reduced respect to WT, compatibly with *p3h1*$^{-/-}$ delay in regeneration (Fig. 2D).

The number of bifurcations was significantly reduced in *Chi*/+ fin rays respect to WT at day 0 and 14 dpa. Interestingly, *p3h1*$^{-/-}$ showed significantly increased number of bifurcations with respect to WT at day 0 and 7 dpa. No difference was observed at 14 dpa, when WT zebrafish reached the same number of bifurcations as *p3h1*$^{-/-}$. No differences in the distance from the first bifurcation to the caudal fin base were detected in both *Chi*/+ and *p3h1*$^{-/-}$ respect to WT (Fig. 2E).

Taken together, these data clearly indicate a defect in the caudal fin morphology of *Chi*/+ and *p3h1*$^{-/-}$ zebrafish. The former is characterized by shorter fin rays that never bifurcate, while the latter has less fin rays with increased number of bifurcations.

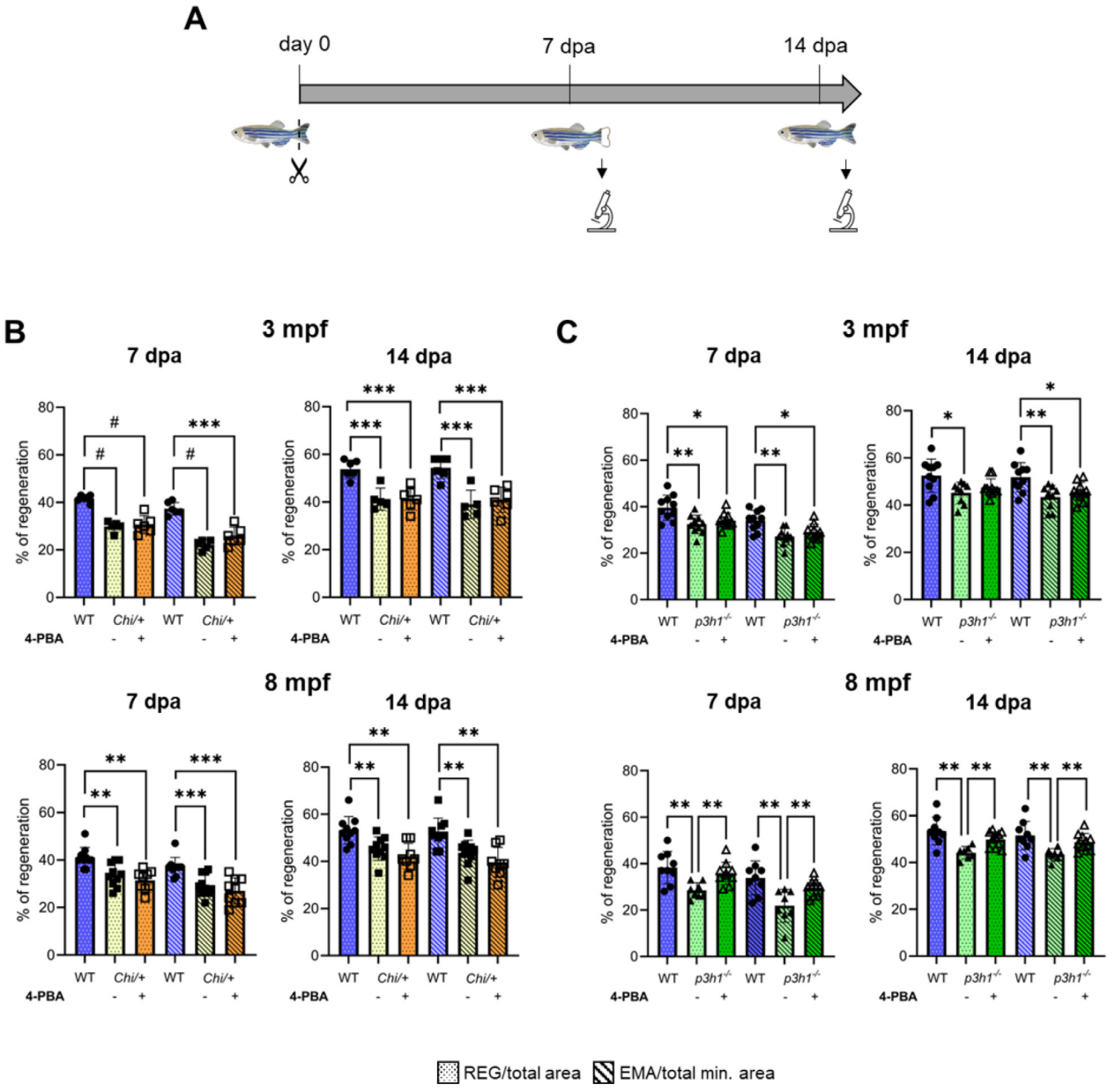

Fig. 1. Caudal fin regeneration is reduced in *Chi*/+ and *p3h1*$^{-/-}$ compared to WT and is rescued by 4-PBA administration only in *p3h1*$^{-/-}$. (A) Caudal fin was amputated and calcein vital staining was performed at 7 and 14 dpa, as shown in the scheme. (B) Caudal fin regeneration of WT and *Chi*/+ siblings. *Chi*/+ zebrafish at 3 and 8 mpf exhibited a significantly reduced caudal fin regeneration compared to WT both at 7 and 14 dpa. 4-PBA treatments did not improve either REG or EMA between controls and treated zebrafish at all ages and time points analyzed (3 mpf: WT $n = 6$, *Chi*/+ controls $n = 5$, treated *Chi*/+ $n = 6$; 8 mpf: WT $n = 10$, *Chi*/+ controls $n = 10$, treated *Chi*/+ $n = 8$). (C) Caudal fin regeneration of WT and *p3h1*$^{-/-}$ siblings. *p3h1*$^{-/-}$ mutants at 3 and 8 mpf showed a significantly reduced caudal fin regeneration compared to WT. 4-PBA administration significantly increased REG and EMA parameters in 8 mpf treated respect to controls, reaching WT value (3 mpf: WT $n = 10$, *p3h1*$^{-/-}$ controls $n \geq 9$, treated *p3h1*$^{-/-}$ $n = 10$; 8 mpf: WT $n = 9$, *p3h1*$^{-/-}$ controls $n \geq 7$, treated *p3h1*$^{-/-}$ $n = 10$). dpa: days post amputation; mpf: months post fertilization; REG: Regenerated Area; EMA: Estimated Mineralized Area. Each dot represents a single value: circle for WT, full square for *Chi*/+ controls, empty square for treated *Chi*/+, full triangle for *p3h1*$^{-/-}$ controls and empty triangle for treated *p3h1*$^{-/-}$. * $P < 0.05$, ** $P < 0.01$, *** $P < 0.001$, # $P < 0.0001$.

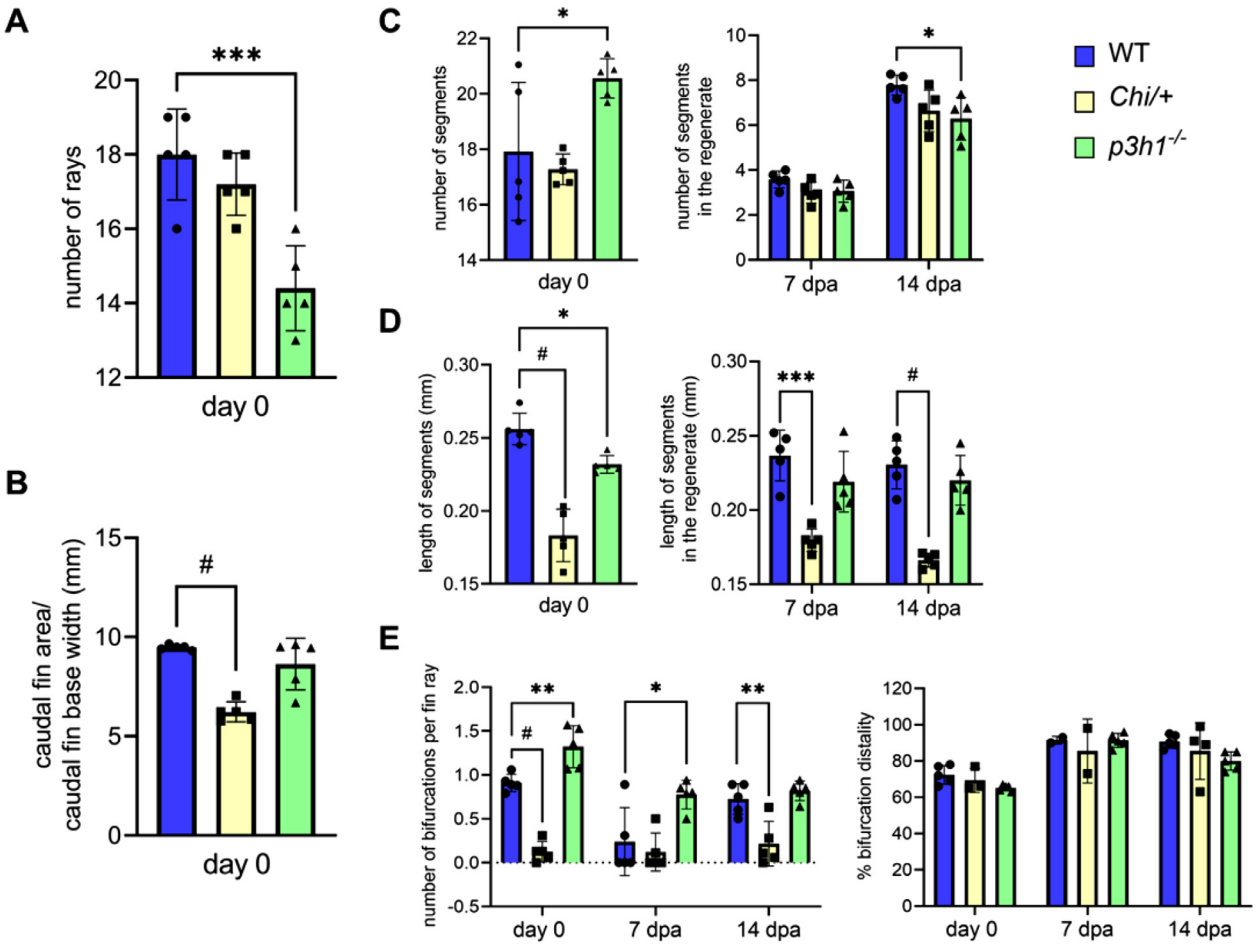

Fig. 2. Morphometric analysis of WT, *Chi*/+ and *p3h1*$^{-/-}$ caudal fin before and during regeneration. Number and length of segments were measured in the total caudal fin at day 0 and only in the regenerated fin at 7 and 14 dpa. (A) A general reduction in the number of rays was detected in *p3h1*$^{-/-}$ compared to WT. (B) Caudal fin area, normalized to the fin base width, was significantly reduced in *Chi*/+ respect to WT. (C) At day 0 the number of segments, increased in *p3h1*$^{-/-}$ with respect to WT, was reduced in the 14 dpa regenerate, compatibly with overall reduced bone formation. (D) The medium length of segments was reduced in *p3h1*$^{-/-}$ respect to WT at day 0 and in *Chi*/+ respect to WT before and during regeneration. (E) *p3h1*$^{-/-}$ zebrafish presented an increased number of bifurcations at day 0 and 7 dpa, while *Chi*/+ rays had significantly less bifurcations at day 0 and at 14 dpa respect to WT. No differences were found in the bifurcation distality percentage, measured as the ratio between the distance to the first bifurcation and the fin ray length, between all zebrafish (n = 5 for each genotype). dpa: days post amputation. Each dot represents a single value: circle for WT, square for *Chi*/+ and triangle for *p3h1*$^{-/-}$. * $P < 0.05$, ** $P < 0.01$, *** $P < 0.001$, # $P < 0.0001$.

Early osteoblast differentiation is not affected during caudal fin regeneration in OI

The key osteoblastogenic differentiation pathways are conserved during zebrafish caudal fin regeneration [25]. To explore in depth the molecular basis of impaired caudal fin regeneration in the two OI zebrafish models, early differentiation was evaluated through RT-qPCR analysis of RNA extracted from caudal fin pools from WT, *Chi*/+ and *p3h1*$^{-/-}$. Differently from the morphometric analysis, in which the 7 and 14 dpa time points were selected to better visualize caudal fin morphology at half regeneration and at a later stage [26], the time points selected for the gene expression analysis were day 0 (basal state), 3 dpa (when early differentiation markers are strongly expressed in the caudal fin [27,28]), and 5 dpa (when late markers start to be expressed [19]), in order to better evaluate possible delays in differentiation (Fig. 3A-B). The expression of the master osteoblastogenic marker *runx2*, duplicated in zebrafish as two paralogues *runx2a* and *runx2b*, and *sox9*, involved in mesenchymal condensation and also duplicated in two isoforms *sox9a* and *sox9b*, were evaluated as the two main markers of early osteoblastogenesis.

In both WT and mutant zebrafish the level of *runx2a, sox9a* and *sox9b* increased at 3 dpa, during the early regenerative process, and showed a decreasing trend at 5 dpa, with the exception of

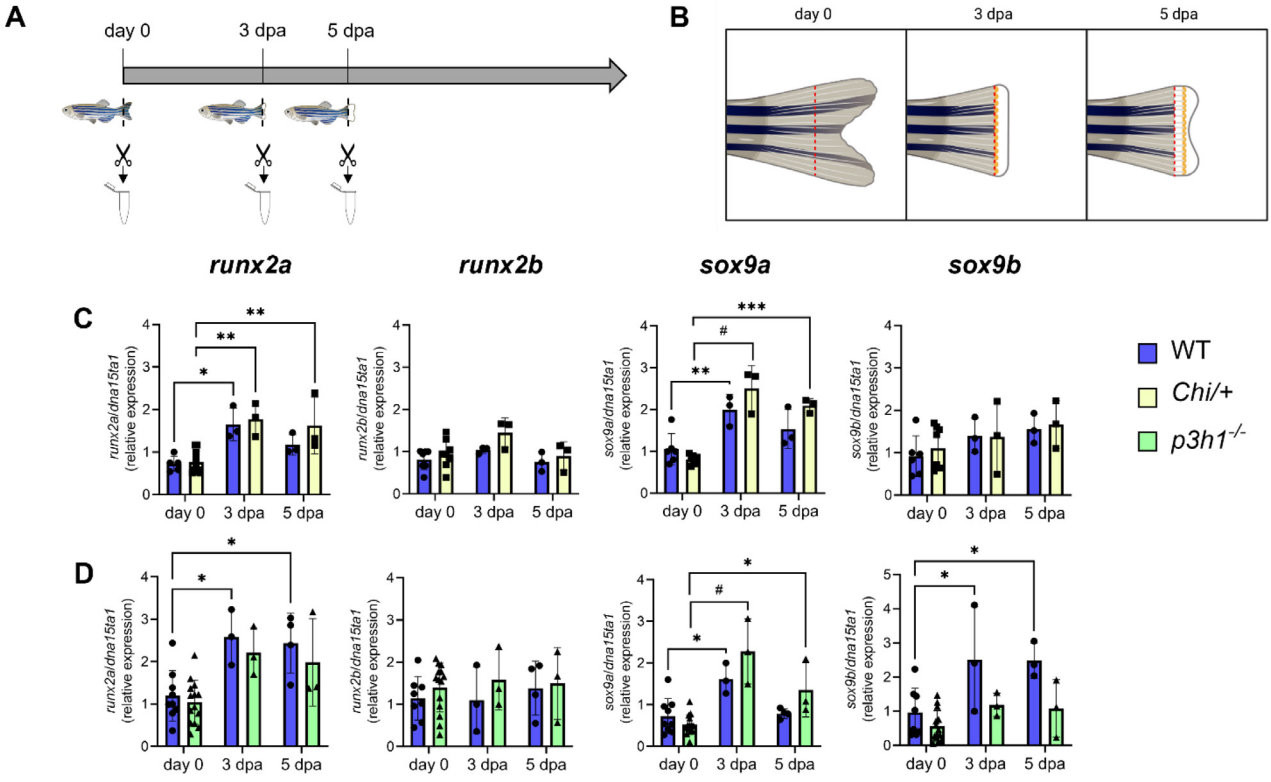

Fig. 3. Sample collection and gene expression analysis of the early differentiation markers *runx2a, runx2b, sox9a* and *sox9b* in WT and mutants. (A) RNA was collected from pools of six caudal fins at day 0, 3 and 5 dpa as shown in the scheme. (B) Detailed schematic view of collected caudal fin samples. Day 0 refers to the portion of the caudal fin obtained after the first amputation at basal state; 3 dpa and 5 dpa regenerates were collected above the amputation plane. Created with BioRender.com. (C) RT-qPCR analysis in WT and *Chi*/+ zebrafish. *runx2a* and *sox9a* showed a significant increase after amputation, with no difference among genotypes. (D) RT-qPCR analysis in WT and $p3h1^{-/-}$ revealed the same trend observed in the previous group. $n \geq 3$ pools of caudal fins for each genotype. dpa: days post amputation. Each dot represents a single value: circle for WT, square for *Chi*/+ and triangle for $p3h1^{-/-}$. * $P < 0.05$, ** $P < 0.01$, *** $P < 0.001$, # $P < 0.0001$.

sox9b that stayed upregulated (Fig. 3C-D). On the contrary, the expression levels of *runx2b* did not show any variation among time points and genotypes analyzed.

Taken together, these data supported normal early osteoblastogenic differentiation in OI *Chi*/+ and $p3h1^{-/-}$ zebrafish.

Osteoblast differentiation is impaired in dominant *Chi*/+ but not in recessive $p3h1^{-/-}$

Osteoblast differentiation upon cell commitment was first investigated by RT-qPCR gene expression analysis of the early-intermediate marker *sp7/osterix* and the late marker *bglap/osteocalcin.* An *in vivo* analysis of the expression of the same markers was then undertaken by confocal microscopy on the mutants crossed with the transgenic zebrafish lines *sp7*:GFP and *bglap*:GFP. The number of GFP+ cells and GFP intensity and distribution within the segments and in the regenerated rays were evaluated. The study was performed at day 0 and at 3 and 5 dpa except for *bglap*, that was not investigated at 3 dpa due to its low expression at this time point.

In both *Chi*/+ and WT zebrafish *sp7* mRNA started to increase at 3 dpa compared to day 0 as expected [19], but no difference was detectable between mutant and WT at any of the analyzed time points (day 0: $p = 0.15$, 3 dpa: $p = 0.18$, 5 dpa: $p = 0.38$) (Fig. 4A). Interestingly, in *Chi*/+; *sp7*:GFP a significant increased number of GFP+ cells was evident in the ray segments at 0 and 3 dpa with respect to WT (Fig. 4B). At the latter time point an accumulation of *sp7*:GFP+ cells at the tip of the regenerating fin rays in mutants was detected (Fig. 4C). No significant difference was found at 5 dpa (Fig. 4B-C). Similar results were obtained by GFP intensity measurements, as *sp7*: GFP signal was significantly increased in *Chi*/+ compared to WT at day 0 and at 3 dpa, even if *sp7*:GFP intensity at the tip of the regenerating rays was still higher in mutants respect to WT (Supplementary Fig. 4A).

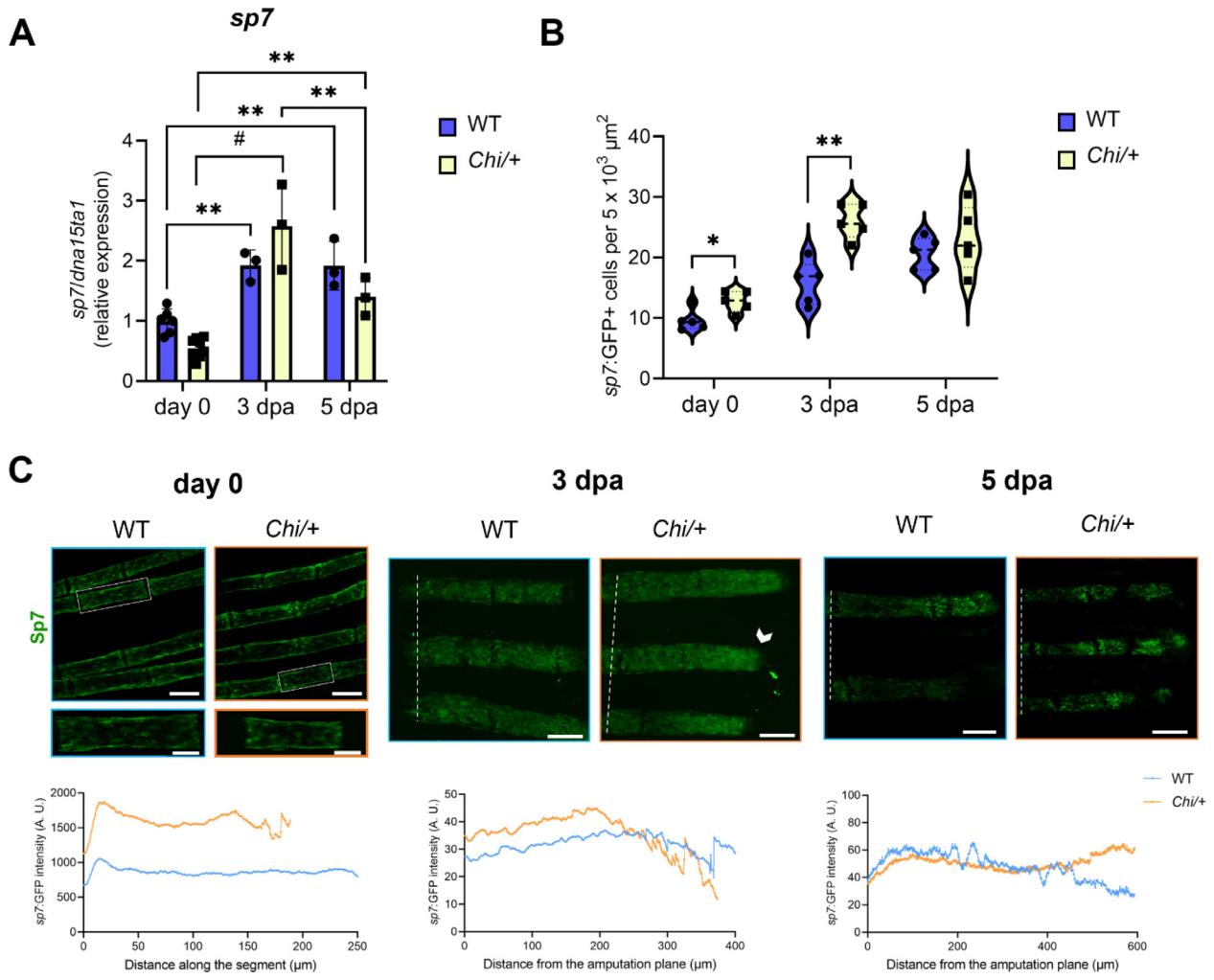

Fig. 4. *sp7* expression analysis in *Chi*/+ and WT caudal fins. (A) RT-qPCR analysis showed increased expression of *sp7* at 3 dpa and decreased level at 5 dpa in both WT and mutant. No differences in *sp7* expression between genotypes ($n \geq 3$ pools of six caudal fins for each genotype) were detected. dpa: days post amputation. (B) *sp7*:GFP+ cells were increased in number at day 0 and 3 dpa in *Chi*/+ respect to WT ($n = 5$ zebrafish for each genotype). (C) Representative images of *sp7*:GFP localization in the fin rays of WT and *Chi*/+ at day 0, 3 and 5 dpa. For each time point is indicated the corresponding distribution analysis (GFP distribution along the segment at day 0, and from the amputation plane at 3 and 5 dpa). No significant differences were found between WT and *Chi*/+, but an accumulation of *sp7*:GFP+ cells could be observed at the tip of the fin rays at 3 dpa (arrowhead). The amputation plane is indicated by the white dotted line. Scale bar: 100 µm. In the graphs, each dot represents a single value: circle for WT and square for *Chi*/+. * $P < 0.05$, ** $P < 0.01$, # $P < 0.0001$.

The expression of *bglap* was significantly reduced in *Chi*/+ with respect to WT at day 0 (Fig. 5A). This result was confirmed by confocal microscopy. Indeed, *Chi*/+*; bglap*:GFP showed decreased number of GFP+ cells in the ray segments at day 0 with respect to WT (Fig. 5B). At this time point, the analysis of GFP distribution inside fin ray segments showed an homogeneous distribution of GFP signal along the segments in WT, while *Chi*/+ presented an accumulation of *bglap*:GFP+ cells in the center of the segments (Fig. 5C). RT-qPCR did not reveal differences between WT and mutant in *bglap* expression at 5 dpa (Fig. 5A), but *bglap*:GFP+ cells were significantly increased in *Chi*/+ with respect to WT, and interestingly an intensity peak of GFP signal was detected at the level of the amputation plane (Fig. 5B-C). Coherently with these results, the overall *bglap*:GFP intensity was found to be significantly decreased at day 0 and increased at 5 dpa in *Chi*/+ with respect to WT (Supplementary Fig. 4B).

Taken together, these data indicate an increased number of immature osteoblasts and a reduction of mature osteoblasts both in the amputated and regenerated caudal fin rays in *Chi*/+ compared to WT, supporting a delay in osteoblast differentiation.

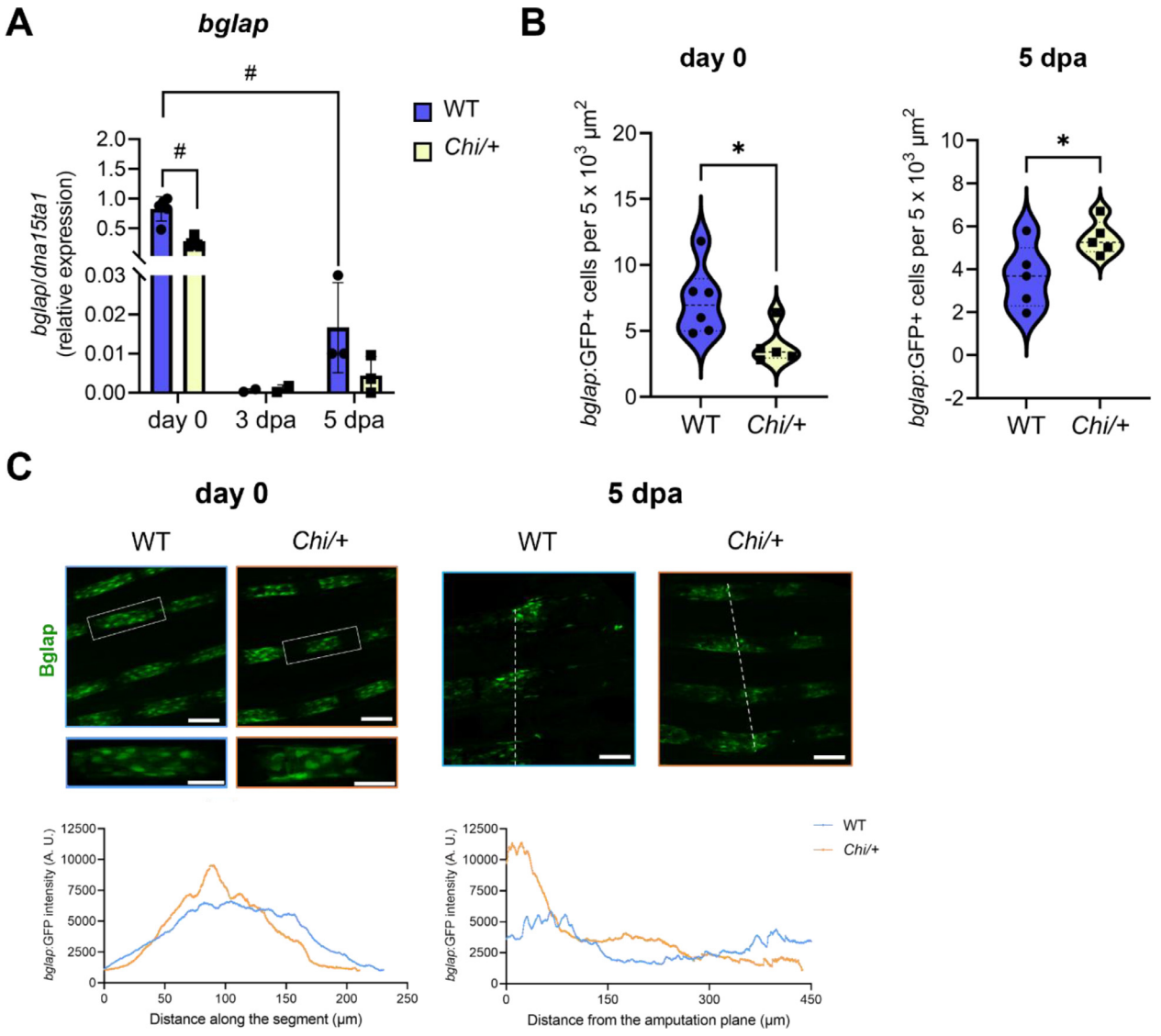

Fig. 5. *bglap* expression analysis in *Chi*/+ caudal fins. (A) RT-qPCR analysis revealed a reduction in *bglap* expression in *Chi*/+ respect to WT at day 0 ($n \geq 3$ pools of six caudal fins for each genotype). For 3 dpa *bglap* expression, 2 pools were used due to low expression level. dpa: days post amputation. (B) The number of *bglap*:GFP+ cells was decreased at day 0 and increased at 5 dpa in *Chi*/+ respect to WT ($n \geq 5$ zebrafish for each genotype). (C) Representative images of *bglap*:GFP localization in the fin rays of WT and *Chi*/+ at day 0 and 5 dpa. For each time point is indicated the corresponding distribution analysis (GFP distribution along the segment at day 0, and from the amputation plane at 5 dpa). At day 0, *bglap*:GFP+ cells accumulated in the middle of the segment in *Chi*/+. At 5 dpa, a peak of *bglap*:GFP+ cells in *Chi*/+ respect to WT, was detected at the level of the amputation plane. The amputation plane is indicated by the white dotted line. In the graphs, each dot represents a single value: circle for WT and square for *Chi*/+. Scale bar: 100 µm. * $P < 0.05$, ** $P < 0.01$, # $P < 0.0001$.

No change in *sp7* and *bglap* expression was detected in *p3h1*$^{-/-}$ at any time points. Coherently with these results, *p3h1*$^{-/-}$*; sp7*:GFP and *p3h1*$^{-/-}$*; bglap*:GFP presented a similar number of GFP+ cells, GFP intensity and distribution compared to WT siblings, indicating normal osteoblast differentiation in this model (Supplementary Figs. 4C-D, 5, 6).

Chi/+ caudal fin shows an increased number of adipocytes

Impaired osteoblast differentiation in dominant OI was previously associated to increased adipogenesis [8], thus adipocytes were evaluated in *Chi*/+ caudal fins at day 0, the time point in which delayed osteoblast differentiation was stronger, as well as in

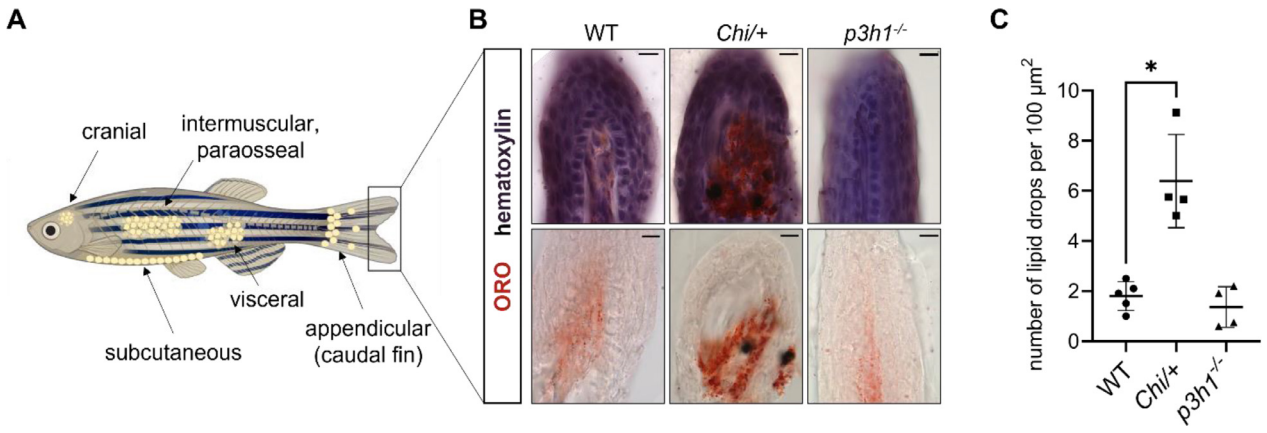

Fig. 6. Adipocytic differentiation in the distal extremity of the caudal fin. (A) Representative images of adipocyte localization in zebrafish. Adipocytes can be found in the cranium, in the viscera, and in the subcutaneous, intermuscular and paraosseal tissues. Appendicular adipocytes were also described in the caudal fin base; *vice versa*, in the distal extremity of the caudal fin, few or no adipocytes should be present. Created with BioRender.com. (B) Oil Red O (ORO) and hematoxylin counterstaining of WT (n = 5), *Chi*/+ (n = 4) and *p3h1*$^{-/-}$ (n = 4) longitudinal caudal fin sections. Double staining on the top, ORO staining on the bottom. Scale bar: 10 μm. (C) Quantification of the number of ORO-stained lipid drops in the distal caudal fin revealed an increased adipogenesis in *Chi*/+ zebrafish. Each dot represents a single value: circle for WT, square for *Chi*/+ and triangle for *p3h1*$^{-/-}$. * $P < 0.05$.

p3h1$^{-/-}$, in which no compromised osteoblast differentiation was proved. Oil Red O (ORO) staining on longitudinal caudal fin sections was undertaken focusing on the most-distal part of the fin, where less adipocytes should be present in normal conditions [29]. While the number of ORO-stained lipid drops was low and did not differ between WT and *p3h1*$^{-/-}$, it was significantly increased in *Chi*/+, proving a switch toward adipogenesis during precursor cells differentiation (Fig. 6).

Osteoclast activity is reduced in mutant caudal fin regenerates

Bone homeostasis requires together with the activity of osteoblasts, responsible for bone formation, also the presence of osteoclasts, driving bone resorption. Zebrafish and mammal bones are subjected to bone resorption thanks to the presence of osteoclasts and the same osteoclastogenic markers are conserved between teleosts and mammals [30]. To study bone resorption in *Chi*/+ and *p3h1*$^{-/-}$ mutants, we investigated both the expression at the transcript level and the enzymatic activity of Tartrate-Resistant Acid Phosphatase (TRAP), a well-known osteoclast marker.

The expression level of *acp5a*, encoding TRAP, was investigated at day 0 and 5 dpa by RT-qPCR. *acp5a* level was significantly increased in WT, *Chi*/+ and *p3h1*$^{-/-}$ after amputation. No differences were detected between genotypes at day 0. Interestingly, a significantly decreased expression level of the gene was detected in *Chi*/+ at 5 dpa respect to WT (Fig. 7A). On the contrary, the *acp5a* expression level in *p3h1*$^{-/-}$ at 5 dpa was similar to WT (Fig. 8A).

TRAP staining was performed on caudal fins collected at day 0 and at 5 dpa. The number of TRAP+ cells was significantly increased in the caudal fins of *Chi*/+ respect to WT and significantly reduced at 5 dpa (Fig. 7B). On the contrary, *p3h1*$^{-/-}$ showed no differences in the number of TRAP+ cells at day 0 and at 5 dpa (Fig. 8B). The intensity of TRAP signal, measured at the level of the amputation plane, was normal in *Chi*/+ (Fig. 7B), but significantly reduced in *p3h1*$^{-/-}$ compared to WT (Fig. 8B).

Differentiation and activity of osteoclasts are regulated through the expression of Receptor Activator of Nuclear Factor κ B (RANKL) and osteoprotegerin (OPG) by osteoblasts. The *rankl* expression level was increased in WT and in both mutants at 5 dpa compared to day 0, whereas no difference was detectable in *opg* level. The *rankl*/*opg* ratio was similar in WT and both mutants at day 0 and 5 dpa (Figs. 7C and 8C). Interestingly, *rankl*/*opg* ratio was significantly increased at 5 dpa respect to day 0 in WT and *p3h1*$^{-/-}$, but not in *Chi*/+ zebrafish.

These data supported a higher presence and activity of osteoclasts only in the *Chi*/+ caudal fin. Furthermore, these results pointed to a reduced number and activity of osteoclasts during regeneration in *Chi*/+ and to a reduced osteoclast migration to the site of amputation in *p3h1*$^{-/-}$.

Considering the differences in the number of bifurcations that we observed in our mutants with respect to WT by morphometric analysis and the association recently described by Cardeira-da-Silva et al. at 7 dpa between bifurcation and osteoclast activity [31], we additionally performed the TRAP assay in both our mutants at this time point. As expected, a tendency towards reduced TRAP staining was still

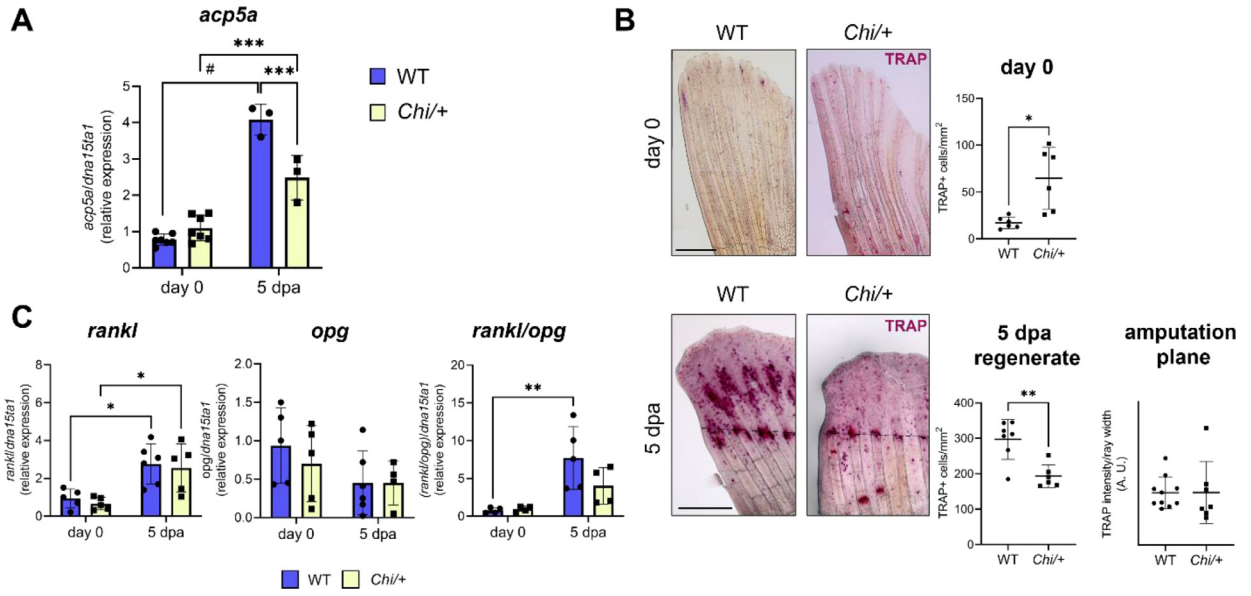

Fig. 7. Osteoclast expression and activity in *Chi*/+. (A) RT-qPCR analysis of *acp5a* expression at day 0 and 5 dpa revealed a reduced transcript expression in *Chi*/+ at 5 dpa ($n \geq 3$ pools of six caudal fins for each genotype). (B) TRAP staining of WT and *Chi*/+ caudal fin samples collected at day 0 and at 5 dpa (the amputation site is indicated by the black dotted line). Osteoclast activity was increased at day 0 and reduced at 5 dpa in mutants respect to WT ($n \geq 6$ caudal fins for each genotype, as indicated by the dots). Scale bar: 500 μm. (C) RT-qPCR analysis of *rankl, opg* and *rankl*/*opg* ratio. No significant differences were detected between genotypes ($n \geq 4$ pools of six caudal fins for each genotype). dpa: days post amputation. In the graphs, each dot represents a single value: circle for WT and square for *Chi*/+. * $P < 0.05$, ** $P < 0.01$, *** $P < 0.001$, # $P < 0.0001$.

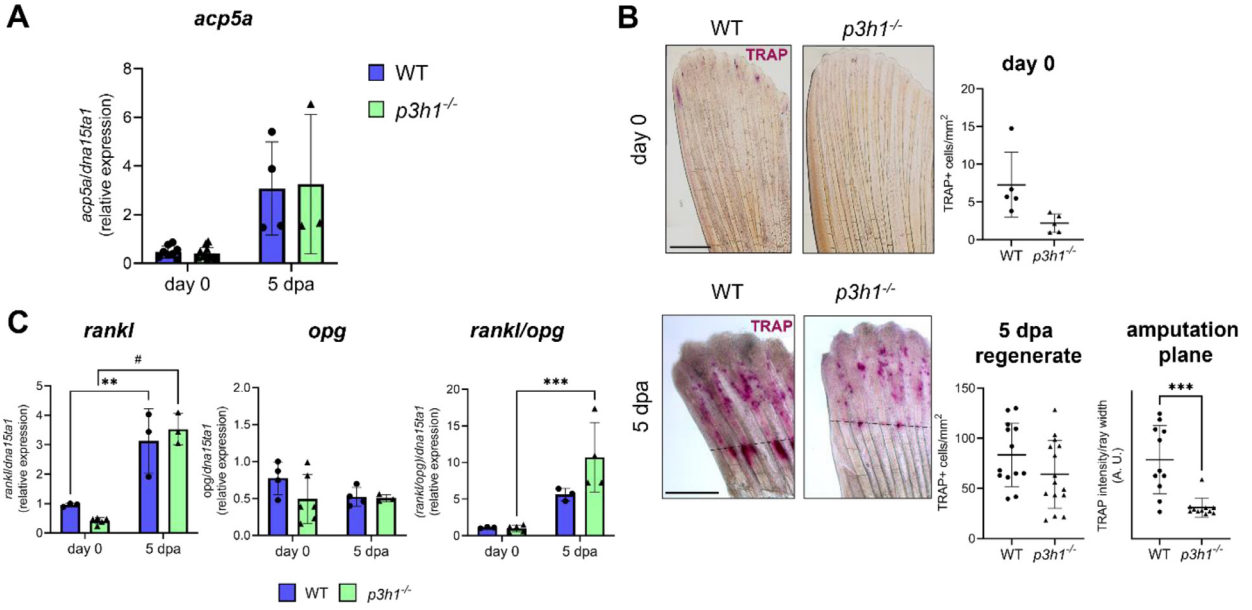

Fig. 8. Osteoclast expression and activity in *p3h1*$^{-/-}$. (A) RT-qPCR analysis of *acp5a* expression at day 0 and 5 dpa showed no differences between genotypes ($n \geq 3$ pools of six caudal fins for each genotype). (B) TRAP staining of WT and *p3h1*$^{-/-}$ caudal fin samples collected at day 0 and at 5 dpa (the amputation site is indicated by the black dotted line). While osteoclast activity of *p3h1*$^{-/-}$ zebrafish was normal at day 0 and in the 5 dpa regenerate, it significantly decreased in the 5 dpa amputation plane with respect to WT ($n \geq 5$ caudal fins for each genotype, as indicated by the dots). Scale bar: 500 μm. (C) RT-qPCR analysis of *rankl, opg* and *rankl*/*opg* ratio. No significant differences were detected between genotypes ($n \geq 3$ pools of six caudal fins for each genotype). dpa: days post amputation. In the graphs, each dot represents a single value: circle for WT and triangle for *p3h1*$^{-/-}$. * $P < 0.05$, ** $P < 0.01$, *** $P < 0.001$.

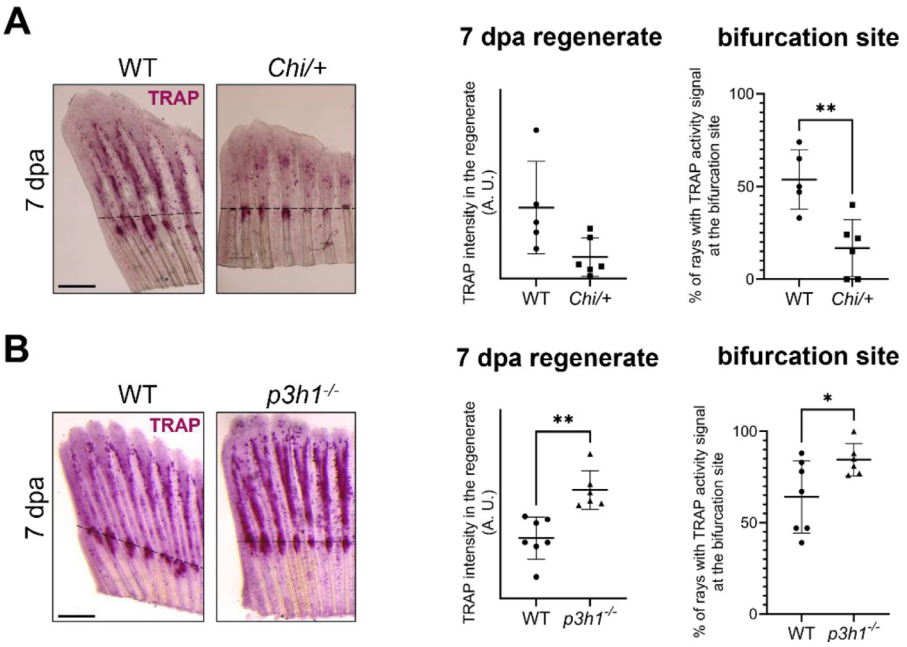

Fig. 9. Osteoclast activity in the regenerate and at the bifurcation site at 7 dpa in WT, *Chi*/+ and *p3h1*$^{-/-}$. (A) TRAP staining of WT and *Chi*/+ caudal fin samples collected at 7 dpa (the amputation site is indicated by the black dotted line). While total TRAP activity in the regenerate was unchanged between WT and *Chi*/+, TRAP signal at the bifurcation site was significantly reduced in *Chi*/+ respect to WT ($n \geq 5$ caudal fins for each genotype, as indicated by the dots). Scale bar: 500 μm. (B) TRAP staining of WT and *p3h1*$^{-/-}$ caudal fin samples collected at 7 dpa (the amputation site is indicated by the black dotted line). TRAP activity was significantly increased in *p3h1*$^{-/-}$ with respect to WT at this time point, with strong TRAP signal detected at the level of the bifurcations ($n \geq 6$ caudal fins for each genotype, as indicated by the dots). Scale bar: 500 μm. * $P < 0.05$, ** $P < 0.01$.

present in *Chi*/+ zebrafish compared to their WT siblings ($p = 0.07$). Furthermore, significantly reduced TRAP signal was detected at the bifurcation site in *Chi*/+ compared to WT, compatible with the reduced number of bifurcations that we observed in this mutant by morphometric analysis (Fig. 9A). The *p3h1*$^{-/-}$ zebrafish, in which we observed a higher number of bifurcations compared to WT at 7 dpa, interestingly showed a significantly increased TRAP signal in the regenerate and at the bifurcation site, suggesting a boost in osteoclast recruitment and differentiation at this time point (Fig. 9B).

Chi/+ caudal fin joint matrix is disorganized

To further investigate the observed morphological alterations in the caudal fin, transmission electron microscopy (TEM) analysis was performed. TEM images of WT joints showed well-organized collagen fibers with a parallel orientation linking consecutive ray segments. The typical collagen banding was clearly visible. On the contrary, *Chi*/+ joints were characterized by a complete disorganization of collagen fibrils, with irregular intersecting directions and lacking the typical collagen banding pattern (Fig. 10A). Furthermore, TEM analysis evidenced the presence of thinner cortex and calli in *Chi*/+ fin rays (Fig. 10B). The structure and the organization of collagen type I fibrils in the caudal fin were also investigated by immunofluorescence. Collagen type I fibrils were distributed parallel to the fin rays and around and inside the caudal fin joints. No difference in collagen general orientation was found between WT and mutants. Nevertheless, in *Chi*/+ some collagen fibril aggregates could be detected as well as an accumulation of fibrils near the fin rays, further demonstrating an impairment in collagen deposition (Fig. 10C).

To deeply address the dysregulation of collagen type I fibrillogenesis, two Fibril-Associated Collagens with Interrupted Triple Helices (FACITs), namely collagen XII and collagen XIV, known to interact with collagen I fibrils [32,33], were investigated by immunofluorescence using antibodies to the zebrafish proteins. Surprisingly, collagen XIV was found to be specifically expressed inside the caudal fin joints, an observation never reported before. Collagen XII was widely distributed in the caudal fin, with its pattern being strongly similar to the one of collagen I fibrils. No abnormalities in the fibril-associated collagen XII deposition were detected in *Chi*/+. Interestingly, collagen XIV fluorescence intensity was significantly higher in mutants and, being strongly expressed at the joint,

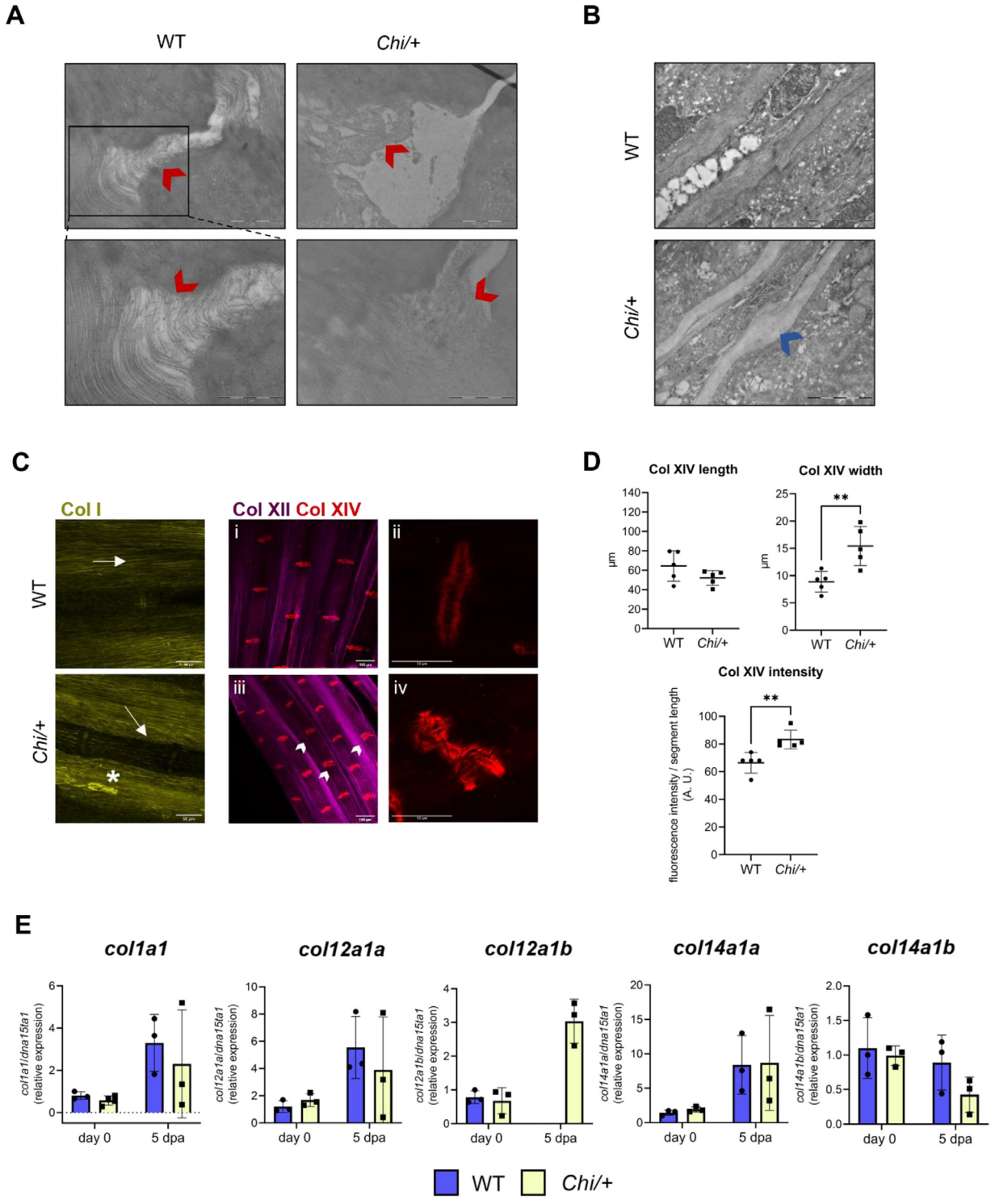

Fig. 10. Collagen disorganization in the caudal fin of *Chi*/+ zebrafish. (A) TEM images of WT (n = 1) and *Chi*/+ (n = 3) collagen fibrils at the caudal fin joints. In the WT several parallel, well organized collagen fibrils connected the inter-joint surfaces. In the mutant, the joint structure appeared disrupted, with fibrils having different orientations and being scattered in the extracellular space, as indicated by the red arrowheads. Scale bar top: 2 μm. Scale bar bottom: 1 μm. (B) TEM images of WT (n = 2) and *Chi*/+ (n = 2) caudal fin rays. The presence of calli along *Chi*/+ fin rays was detected, as indicated by the blue arrowhead. Scale bar: 2 μm. (C) Representative immunofluorescence of collagen I, XII and XIV in WT and *Chi*/+ caudal fin. Collagen I fibrils were thick and parallel to the fin ray in WT (arrow). In *Chi*/+ they accumulated in proximity to the fin ray (arrow), in some cases forming aggregates (asterisk). Collagen XII was distributed widely in the caudal fin, similarly to collagen I. Collagen XIV specifically localized in the fin ray joints. In *Chi*/+, joints showed altered

allowed to appreciate a wider inter-joint space in *Chi*/+ respect to WT (Fig. 10C-D), further supporting the matrix disorganization observed by TEM. Of note, joint deformities in *Chi*/+ were detected also in the regenerating caudal fin at 5 dpa. Nevertheless, a deeper investigation of collagen XIV distribution in 5 dpa transversal caudal fin sections from WT and *Chi*/+ revealed no anomalies in collagen XIV distribution along the fin rays (Supplementary Fig. 7).

To investigate how the reorganization of the caudal fin joints affects the swimming of *Chi*/+ zebrafish, spontaneous swimming behavior was investigated and demonstrated a significant decrease in the total distance travelled by *Chi*/+ zebrafish compared to their WT siblings (Supplementary Fig. 8A) with a significantly increased movement ratio of the caudal fin in *Chi*/+ zebrafish (Supplementary Fig. 8B). The swimming path, plotted in Supplementary Fig. 8C, highlighted a smooth S-shaped curvature of the tail-base in WT zebrafish, whereas a more erratic (spastic), less symmetrical movement of the caudal fin was observed in *Chi*/+. Moreover, *Chi*/+ zebrafish had difficulties to swim straight, and their paths were often more curved compared to the mostly straight swimming path in WT zebrafish (Supplementary Fig. 8D).

RT-qPCR analysis of *col1a1, col12a1a, col12a1b, col14a1a* and *col14a1b* did not show differences in transcript expression among the two genotypes. Interestingly, *col12a1b* expression was detectable in 5 dpa samples only in mutants, but not in WT (Fig. 10E).

Immunofluorescence was also carried out for *p3h1*$^{-/-}$ zebrafish to evaluate collagen network organization. Collagen type I fibrils showed normal orientation in this model, but fibrils appeared wavy and strongly disorganized, with some collagen I signal trapped inside the fin rays. No alterations were detected for collagen XII and XIV (Supplementary Fig. 9).

These data indicated a collagen type I fibril disorganization in both *p3h1*$^{-/-}$ and *Chi*/+ mutants, affecting, only in the latter, which also showed swimming alterations, the secretion and organization of other extracellular matrix collagenous proteins and, ultimately, impairing joint organization.

Discussion

This study shows the suitability of zebrafish caudal fin regeneration analysis to deeply investigate bone cell differentiation and activity in zebrafish models of OI. Here we demonstrate that despite causing intracellular mutant collagen retention and a similar skeletal phenotype, structural mutations in collagen type I have different consequences both at cellular and molecular level compared to mutations in a protein relevant for collagen type I post-translational modification.

The impaired bone formation associated to a delay in growth characterizing individuals affected by OI [34−37] can be easily and quickly investigated *in vivo* in zebrafish taking advantage of their ability to regenerate after amputation the caudal fin that is mainly composed by bony rays and soft tissue [38]. The reduced caudal fin regeneration ability detected in both dominant *Chi*/+ and recessive *p3h1*$^{-/-}$ OI zebrafish models confirmed the delay in their bone formation thus strengthening their value to investigate the OI bone phenotype. To dissect the molecular basis of the impaired bone formation, bone cell differentiation was evaluated. RT-qPCR data highlighted normal early osteoblastogenesis steps in both OI models as demonstrated by normal *runx2a/b* and *sox9a/b* transcript expression. Interestingly, a clear delay in osteoblast maturation and migration was only evident in *Chi*/+ zebrafish. s*p7*+ committed osteoblasts were increased in *Chi*/+ respect to WT up to 5 dpa, when mature osteoblasts are instead expected to be more abundant. Even if the number of *bglap*+ mature osteoblasts was increased in *Chi*/+ respect to WT at 5 dpa, their presence was mainly limited at the amputation site, suggesting a defect in their dedifferentiation. The delay in osteoblasts differentiation was further supported by the analysis performed at day 0, in which only committed osteoblasts were increased whereas the presence of mature osteoblasts was very limited. These findings support *in vivo* the impairment in bone forming cell differentiation reported previously *in vitro* in dominant OI patients as well as in murine models [8−10,39]. It would be interesting to further investigate the spatial distribution of *runx2a* and *sox9a* using transgenic lines as done for *sp7* and *bglap* in future studies. This could provide additional insights into the localization of early osteoblastogenesis markers during fin regeneration and their potential impact on fin patterning and regeneration in OI pathology.

The defective osteoblast differentiation found in *Chi*/+ paired to a significantly increased number of lipid drops at the tip of the caudal fin. This finding, that supports the presence of an osteoblast-

structure and increased inter-joint space, as indicated by the arrowheads (i: collagen XII and collagen XIV co-labeling in WT zebrafish; ii: 63X magnification of collagen XIV-labeled joint in WT zebrafish; iii: collagen XII and collagen XIV co-labeling in *Chi*/+ zebrafish; iv: 63X magnification of collagen XIV-labeled joint in *Chi*/+ zebrafish). (D) Collagen XIV analysis revealed increased joint width and fluorescence intensity in *Chi*/+ respect to WT (n = 5 for each genotype). (E) RT-qPCR analysis of collagens did not show differences between the two genotypes (n = 3 pools of six caudal fins for each genotype). dpa: days post amputation. In the graphs, each dot represents a single value: circle for WT and square for *Chi*/+. ** $P < 0.01$.

adipocyte switch in a zebrafish OI model, strengthens the correlation between impaired osteoblastogenesis and increased adipogenesis *in vivo*, indicating this feature as a characteristic of dominant OI as previously described in *in vitro* experiments, both in OI individuals and murine mesenchymal stem cells (MSCs) [8,40].

On the contrary, *p3h1*$^{-/-}$ zebrafish showed normal bone cell differentiation and no increased adipogenesis, suggesting that in this recessive OI form the defective bone forming cell differentiation does not play a significant role in bone regeneration as in the dominant form of the disease.

High bone turnover due to excessive bone resorption is one of the key features of OI pathology [3]. Osteoblast and osteoclast activity in bone is tightly coupled and mutations causative of OI are frequently associated to an imbalance between bone formation and bone resorption. The number of TRAP+ cells was found to be significantly reduced at 5 dpa in *Chi*/+ with respect to WT. This result was surprising, since to our knowledge this is the first time in which decreased osteoclast activity is described during bone formation in OI. Nevertheless, we should be careful in interpreting these data since bone formation of the dermal caudal fin does not fully recapitulate the formation of the endoskeleton, and the role of osteoclasts in caudal fin regeneration has been still poorly explored.

The osteoblast and osteoclast results support in dominant, but not in recessive OI, a prevalent role of defective osteoblasts and impaired osteoclast activity in causing reduced caudal fin bone formation.

At day 0, the presence of immature osteoblasts failing to express *bglap* is associated to an increased number of TRAP+ cells in *Chi*/+ respect to WT, suggesting that during bone remodeling impaired osteoblast maturation may induce an increase in bone turnover similar to what observed in dominant OI individuals [39] as well as in the *Brtl* mouse [41]. Nevertheless, it must be considered that the fragile *Chi*/+ caudal fins are more prone to fractures, which could partially explain the increase in bone resorption. In *p3h1*$^{-/-}$ caudal fin the level of TRAP+ cells was normal at day 0, in accordance with what found for *P3h1* null mice, characterized by normal osteoblast and osteoclast surfaces [42]. Also, a normal number of osteoclasts was reported *in vivo* and *ex vivo* in the OI type VII murine model *Crtap*$^{-/-}$, which is phenotypically and biochemically similar to the *P3h1* null mice [43].

We did not detect any variation in the expression levels of *rankl* and *opg* nor in the *rankl*/*opg* ratio in both OI zebrafish, similarly to what reported for the *Brtl* mouse [41], confirming that the impaired osteoclastogenesis found in the two models is not directly linked to the Rankl/Opg axis.

Of interest, a reduced TRAP signal at the amputation plane was evident in *p3h1*$^{-/-}$ compared to WT zebrafish. We recently described an increased TRAP staining signal at the level of the amputation plane, linked to an increased expression of the macrophage precursor marker *mpeg1* in the regenerating caudal fin of the zebrafish mutant for OI type XIV *tmem38b*$^{\Delta 120-7/\Delta 120-7}$, indicating the recruitment of precursors that failed to differentiate [22]. The low signal at the amputation plane in *p3h1*$^{-/-}$ may indicate a compromised recruitment and migration to the remodeling site. Lack of 3-hydroxylation not only alters the extracellular matrix composition but can also negatively affect the activity of proteins involved in bone metabolism. Among these, the hypoxia-inducible factor HIF-1α turnover is regulated by prolyl hydroxylation, that triggers binding and ubiquitination via the proteasome [44]. Multiple works demonstrated that constitutively active HIF-1α by prolyl hydroxylase inhibition reduces osteoclasts number and activity *in vitro* [45,46]. Furthermore, a disruption in *HIF-1*α-regulated factors operating in cytoskeleton dynamics was detected in fibroblasts from OI individuals affected by *CRTAP, P3H1* and *PPIB* mutations [47]. Zebrafish HIF-1α, known to be involved in macrophage mobilization [48], can undergo 3-prolyl hydroxylation (source: Uniprot). Thus, we speculate that lack of 3-hydroxylation may alter HIF signaling leading to osteoclast defect in our model. Deeper study of this mechanism was beyond the scope of this paper, but it would indeed be worth future investigation.

Recently, it was demonstrated that caudal fin ray bifurcation depends on a fine-tuned balance between bone formation and bone resorption, in which TRAP+ osteoclasts play a role in defining branchpoint position [31]. Our morphometry results seem to indicate that *p3h1*$^{-/-}$ rays bifurcate early in time with respect to WT. Indeed, most of the bifurcations were already present at 7 dpa in *p3h1*$^{-/-}$, whereas WT reached the same number later at 14 dpa. The low TRAP signal observed in the 5 dpa amputation plane of *p3h1*$^{-/-}$ supports a delay in osteoclast precursors recruitment at the remodeling site, followed by their catch up at 7 dpa when we observed an increased TRAP staining in the regenerate and the bifurcation site, indicating a “boost” in osteoclast recruitment at this time point. In a similar way, the reduced number of bifurcations in *Chi*/+ went together with a reduced TRAP signal at the bifurcation site. Nevertheless, the branchpoint position with respect to the amputation plane was unchanged in both our mutants with respect to WT. We speculate that in *Chi*/+ this is the result of impaired osteoblast differentiation and osteoclast activity, whereas in *p3h1*$^{-/-}$ it is possible that the impairment in osteoblast activity revealed by the delay in regenerate growth overcomes the disturbance of osteoclast recruitment and activity.

An important question we tried to address was also the consequence of mutant extracellular matrix

in the caudal fin of our OI zebrafish models. We previously reported the presence of overmodified collagen and impaired fibril assembly in bone and skin of adult *Chi*/+ and *p3h1*$^{-/-}$. Here we demonstrated a disorganized collagen type I deposition in the caudal fin in both models, in some cases with the formation of aggregates typical of misfolded proteins.

In order to further investigate fibril organization, we focused our attention on two well-known FACITs involved in collagen type I fibrillogenesis, collagen types XII and XIV. For the first time, we described specific localization of collagen type XIV in the joints of the zebrafish caudal fin, making this collagen a unique marker of the joints. This could be coherent with the fact that collagen XIV mainly localizes in dense connective tissues, such as tendons [49]. Collagen XIV is transiently expressed during early stages of development [32,50] and during caudal fin regeneration [51]. Collagen XII is more widely and constantly expressed during development, maturation and aging in most connective tissues [33,52,53]. We indeed observed collagen XII to be widely and regularly distributed along the caudal fin and inside the fin ray segments and joints. Collagen XII may replace collagen XIV during development or regeneration, as others already suggested [32], explaining its spreader localization inside the caudal fin.

Transmission electron microscopy analysis of *Chi*/+ caudal fin joints showed disorganized collagen I fibrils, which by immunofluorescence investigation resulted associated to an increase in collagen XIV amount. An increased inter-joint space before and during regeneration was evident in *Chi*/+. No abnormalities were on the contrary detected in *p3h1*$^{-/-}$ zebrafish. It is tempting to speculate that these differences are due to the extracellular matrix composition of the two models. In *Chi*/+ the mutant collagen consists of a mix of molecules with one (50%), [redacted] (25%) or none (25%) mutant chains [54], where [redacted] *p3h1*$^{-/-}$ zebrafish, only mutant molecules are [redacted] duced. The collagen heterogeneity in *Chi*/+ may differentially impact the interaction with other proteins and collagens involved in fibrillogenesis, as already reported to modulate the skeletal severity in the *Brtl*/+ and *Brtl*/*Brtl* mice [55].

No difference in the expression of *col1a1, col12a1a, col14a1a/b* was found whereas *col12a1b*, usually absent in the WT, being a later expressed gene [50], was present in mutant regenerates. However, lack of specific antibody for this isoform complicated its investigation at the protein level. Further studies, that are beyond the purpose of the present investigation, will be required to clarify the role of the two FACITs in the caudal fin, their timely activation and their specific localization.

Interestingly, the defective caudal fin joints in *Chi*/+ link impaired altered collagen fibrils to abnormal swimming behavior as demonstrated by shorter swim paths and fin erratic movements in mutants respect to WT. Nevertheless, it should be taken into account that in addition to the fin phenotype, the swimming behavior in *Chi*/+ zebrafish could also be affected by alterations in the axial skeleton.

The mutations in *col1a1a* and in *p3h1* respectively have different consequences on caudal fin morphometry, likely pointing to the peculiar function of the structural *versus* enzymatic defects. The most striking observation was the reduced number of fin rays in the *p3h1*$^{-/-}$ model compared to WT (17.80 $\pm$ 1.64 versus 14.40 $\pm$ 1.14, $p < 0.01$). This finding supports a defect in the cartilaginous plates strengthening the role of P3h1 protein on cartilage structures already reported in murine OI models [37,43] and in the notochord of the zebrafish *p3h1*$^{-/-}$ [7]. Indeed, fin rays derive from endochondral hypurals located at the end of the zebrafish body and during zebrafish larval development, two cartilaginous plates constituted by hyaline-cell cartilage containing elastin fibers, cover the distal ends of hypurals to support the unidirectional formation of mineralized rays [56–58].

In presence of the same number of fin rays, in *Chi*/+ the length of the segments was instead reduced since day 0 and throughout regeneration likely due to the collagen defect in this model. It was previously demonstrated how collagen mutations impact collagen-rich structures such as the fin rays. For instance, the zebrafish *prp* carrying mutation in collagen IX shows wavy fin rays associated to an altered osteoblast localization [59], a phenotype shared with *Chi*/+. *Chi*/+ regenerating caudal fin failed to synthesize the actinotrichia, collagenous structures localized at the distal extremity of the fin rays and involved in fin ray morphogenesis [60,61]. Our current results strengthen this interpretation by linking collagen and actinotrichia defects to impaired [redacted]ray segmentation.

[redacted]Nowadays no cure is available for OI and new [redacted]atments to ameliorate quality of life of patients are urgently needed. Drug repositioning allows to test already FDA approved drugs on different diseases, including several skeletal dysplasias [62–64]. Among these, 4-phenylbutyrate (4-PBA), an ammonia scavenger for the treatment of urea cycle disorders, has recently become of increasing interest in the OI field due to its chemical chaperone activity. Indeed, it was recently demonstrated that *in vitro* 4-PBA ameliorates OI cell homeostasis by reducing unfolded protein response, activating autophagy and reducing apoptosis both in dominant and recessive forms of the disease, both in primary fibroblasts and osteoblasts [6,65,66].

In this study we demonstrated that treating *p3h1*$^{-/-}$ with 4-PBA significantly increased bone growth during caudal fin regeneration both at 7 and 14 dpa as demonstrated by the rescue of REG and EMA parameters, with a significant effect only on 8 mpf adult zebrafish. Interestingly, despite no effect of

developmental stage on caudal fin regeneration ability was observed in the current study, we previously showed that *p3h1*$^{-/-}$ zebrafish phenotype generally worsens with age, with increased number of fractures in the ribs and vertebral compressions in adult zebrafish [7]. This may support the accentuated effect of 4-PBA in older zebrafish which have a more compromised phenotype and thus can benefit more from the drug administration.

On the contrary and unexpectedly, no effect on bone formation was detected on 4-PBA treated *Chi*/+ at both 3 and 8 mpf. In a previous study on adult *Chi*/+, we observed a positive effect of the drug in stimulating collagen secretion in the matrix during caudal fin regrowth [17]. Our present results suggest that the increase of mutant collagen in the extracellular matrix may not be enough to ameliorate bone formation. Nevertheless, also *p3h1*$^{-/-}$ collagen type I has an altered structure, thus the question on why in the two models the effect of 4-PBA is different is quite intriguing. Although we do not have a final answer, we reasoned on three hypotheses. First, as previously described, the heterogeneity of *Chi*/+ collagen compared to the homogeneous *p3h1*$^{-/-}$ collagen could play a role. A more appealing second hypothesis is that in *Chi*/+ we observed reduced number of mature osteoblasts, which are the target cells of 4-PBA during bone regrowth. It is possible that the amount of secreted collagen upon chaperone administration is not enough to improve bone formation in this model. Finally, 4-PBA effect may be dependent on the type of ossification. In our previous work, despite improved mineralization was proved in several cranial bones in *Chi*/+ larvae, no effect was detected in the cleithrum, which has a dermal origin as the caudal fin [17]. We cannot anyway exclude a gene mutation-specific effect of 4-PBA *in vivo* as already suggested from *in vitro* studies on OI patients' fibroblasts [65].

No effects of 4-PBA were detected on gene expression of bone cell differentiation markers in both *Chi*/+ and *p3h1*$^{-/-}$, suggesting that the positive effect of 4-PBA on cellular homeostasis is not due to its known histone deacetylase inhibitor activity [67].

The relevance of our results is strengthened by their possible translation to better dissect the cell differentiation occurring during injury repair in humans. Indeed, most long bone fractures heal by a combination of intramembranous and endochondral ossification, both requiring a programmed cell commitment. The same bone cell types that we investigated in caudal fin regeneration experiments, are the ones differentiating and necessary for fin ray fracture repair [68,69]. Based on the delay in osteoblast differentiation and osteoclast activity in *Chi*/+, it is tempting to speculate a similar defect in an injury model.

In conclusion, we investigated bone morphology, bone cellular and molecular patterning, and matrix assembly in two zebrafish models of OI using the caudal fin as a tool. For the first time we provide a direct experimental comparison between two models of the disease with different molecular defects: *Chi*/+, characterized by a collagen defect resulting in dominant OI, and *p3h1*$^{-/-}$, affected by an enzymatic defect leading to recessive OI. We demonstrated that caudal fin regeneration is similarly impaired in both dominant and recessive OI. Nevertheless, only the structural defect in collagen type I has a negative effect on osteoblast differentiation that results in a switch towards the adipocytic lineage, already reported *in vitro* for dominant OI, but never *in vivo*. Osteoclast impairment during caudal fin regeneration that recapitulates bone formation in zebrafish is reported for the first time in both dominant and recessive OI zebrafish models independently from the Rankl/Opg axis. The administration of the chemical chaperone 4-PBA rescues caudal fin regeneration in *p3h1*$^{-/-}$, demonstrating for the first time its beneficial effect on recessive OI *in vivo*.

Materials and methods

Zebrafish husbandry and ethical statement

AB wild-type zebrafish used for this study were obtained from the European Zebrafish Research Center (EZRC). The mutant *Chi*/+ carrying a G2207A mutation in *col1a1a*, causing a p.G736D (G574D) substitution in the α1 chain of type I collagen, was originally provided by Prof S. Fisher (Boston University, USA). The mutant *p3h1*$^{-/-}$, carrying a c.645delCinsGGAGAA deletion resulting in a stop codon, was previously generated in our laboratory [7]. Other lines used in this study were *Tg(Ola.bglap:EGFP)*^{hu4008} (referred as *bglap:GFP*) [70] and *Tg(OlSp7:nlsGFP)*^{zf132} (referred as *sp7:GFP*) [71]. Zebrafish embryos were kept in petri dishes until 6 days post fertilization (dpf) in zebrafish water (1.2 mM $NaHCO_3$, 0.1 g/L instant ocean, 1.4 mM $CaSO_4$, 0.00002% w/v methylene blue) at 28 °C and then housed in ZebTEC semi-closed recirculation housing systems (Tecniplast) at 28 °C, pH 7.5 and conductivity 500 μS on a 14/10 light/dark cycle. Adult zebrafish were fed three times a day alternating dry food and brine shrimps. For the experiments, larvae and adult zebrafish were anesthetized using 0.016% w/v tricaine (3-amino benzoic acidethylester, Sigma-Aldrich) in zebrafish water and/or sacrificed by tricaine overdose (0.03% w/v). All the experiments were performed in agreement with EU Directive 2010/63/EU. The experimental protocol was approved by Italian Ministry of Health (Approval Animal Protocol No.1191/2016-PR and 260/2020-PR).

Genotyping

Genomic DNA was extracted from caudal fin clip of adult zebrafish. Tissue was digested by proteinase K (2.5 mg/mL, Sigma-Aldrich) in lysis buffer (100 mM Tris−HCl, pH 8.5, 5 mM EDTA, 0.2% w/v SDS, 200 mM NaCl) o/n at 55 °C, followed by precipitation with isopropanol and resuspended in Tris-EDTA Buffer (20 mM Tris−HCl, 1 mM EDTA, pH 8.0) o/n at 55 °C.

PCR amplification of *p3h1* (NC_007122.6) region of interest was carried out using specific primers (FW: 5′-CTACACTAACATGTACATGTATGC-3′ (4748−4771 nt), RV: 5′-ACAGTGTGTATATTCTGCATCCC-3′ (5181−5203 nt)) using 60 °C annealing temperature. The amplicon was digested with Eco0109I (New England BioLabs) and run on 8% v/v acrylamide gel in TBE buffer (0.1 M Tris−HCl, 0.1 M H_3BO_3, 2 mM EDTA, pH 8.2). Two bands of 319 bp and 125 bp were expected in WT zebrafish, while in *p3h1*$^{-/-}$ a single 444 bp band indicated the lack of the restriction site due to the inserted mutation.

Chi/+ genotyping was carried out taking advantage of the fin fold bending present only in mutants starting from 5 dpf [17].

RNA extraction and RT-qPCR

RNA was extracted from a minimum of three pools (detailed number in figure legends) of six caudal fins from each time point from 8 mpf (adult) WT, *Chi*/+ and *p3h1*$^{-/-}$ using QIAzol Lysis Reagent (Qiagen) according to manufacturer's instructions. Contaminant DNA was eliminated using DNA-free kit DNase Treatment & Removal (Invitrogen). RNA quantity was determined by NanoDrop spectrophotometer, and its quality was evaluated by 1% w/v agarose gel electrophoresis in TBE buffer. Reverse-transcription was performed using the High-Capacity cDNA Transcription kit (Applied Biosystems) according to manufacturer's protocol in a final volume of 20 μL. Real time quantitative PCR (RT-qPCR) was used to evaluate gene expression of *runx2a, runx2b, sox9a, sox9b, acp5a, sp7, bglap, rankl, opg, col1a1a, col12a1a, col12a1b, col14a1a* and *col14a1b* in WT and mutant zebrafish. *dna15ta1* was used as reference gene [72]. Primer sequences and annealing temperatures are reported in Supplementary Table 1. RT-qPCR was performed with SYBR Green Master mix (Applied Biosystems) in triplicate in a 25 μL final volume. The RT-qPCR cycle was the following: 2 min of denaturation at 95 °C, 44 cycles of 5 s at 95 °C, 30 s at the annealing temperature followed by 1 second at 72 °C. A dissociation curve was performed starting with 5 s at 95 °C, followed by 1 min at 58 or 60 °C and finally gradual heating to 95 °C at a ramp-rate of 0.11 °C/s to check the specificity of the amplification. The relative expression was calculated using ΔΔCt method. The QuantStudio 3 thermocycler and the QuantStudio Design & Analysis software (Applied Biosystems) were used.

Bone formation evaluation

The caudal fins of 3 and 8 mpf WT, *Chi*/+ and *p3h1*$^{-/-}$ zebrafish were amputated and fin regeneration was evaluated after 7 and 14 days post amputation (dpa). In each experiment, both mutants were matched with their WT siblings. Each zebrafish after amputation was placed in 200 mL of zebrafish water in a bench top tank kept at 26 °C and half of the volume was replaced every day. After 7 and 14 dpa zebrafish were stained for 10 min with a 0.2% w/v solution of calcein (Sigma-Aldrich) and washed until the water was clear to remove unbound dye. Images of 7 and 14 dpa caudal fins were acquired using a Leica M165 FC microscope connected to a Leica DFC425 C digital camera. The regeneration in WT, *Chi*/+ and *p3h1*$^{-/-}$ zebrafish was estimated using two parameters, the Regenerated Area (REG), representing all the regenerated area, including rays and surrounding connective tissue, and the Estimated Mineralized Area (EMA) representing the regenerated mineralized rays and inter-ray spaces. The percentage was determined by measuring the ratios REG/total caudal fin area and EMA/total mineralized caudal fin area [24] (Supplementary Fig. 10).

Caudal fin morphometry

For morphometric analysis caudal fin regeneration assay was performed on WT, *Chi*/+ and *p3h1*$^{-/-}$ zebrafish. Calcein vital staining at day 0, 7 dpa and 14 dpa was performed as described above. Number of fin rays and caudal fin size were evaluated at day 0. At each time point the number and length of segments per ray, the number of bifurcations per ray, the distance from the end of the body to the first bifurcation (indicated as distance to bifurcation in the text) were evaluated. Number and length of the segments were measured in the total caudal fin at day 0 and only in the regenerated portion of the fin at 7 and 14 dpa. Images were acquired both in bright-field and in fluorescence using a Leica M165 FC microscope connected to a Leica DFC425 C digital camera. Measurements were performed using the LAS v4.13 software (Leica). The most lateral, smaller rays were not considered for the analysis.

Tartrate-resistant Acid Phosphatase (TRAP) staining

Tartrate-resistant Acid Phosphatase (TRAP) staining was performed following a published protocol [21]. Caudal fins of adult WT, *Chi*/+ and *p3h1*$^{-/-}$ zebrafish at the time points indicated in the figure

legends were fixed in 4% PFA in PBS o/n at 4 °C, washed in PBT (0.1% v/v PBS + Tween-20) and permeabilized in PBTx (0.3% v/v PBS + Triton X-100). Fins were then equilibrated in TRAP Buffer (0.1 M sodium acetate, 0.1 M acetic acid, 50 mM sodium tartrate) and color reaction was performed in TRAP Buffer containing 0.1 mg/ml Naphtol AS-MX phosphate (Sigma-Aldrich) and 0.3 mg/ml Fast Red Violet LB (Sigma-Aldrich). Fins were finally bleached in 10% H_2O_2 + 1% KOH o/n at RT to remove pigmentation and then stored in 70% glycerol at 4 °C until acquisition. Images were acquired using a Leica M165 FC microscope connected to a Leica DFC425 C digital camera. The number of TRAP+ cells in the amputated and regenerated was counted using the Cell Counter tool of Fiji (ImageJ) software. In the stump, where TRAP signal was more intense, the TRAP area was measured on individual rays and normalized to ray width.

4-phenylbutyrate (4-PBA) treatment

Caudal fins of 3 and 8 mpf WT, *Chi*/+ and *p3h1*$^{-/-}$ zebrafish were amputated and allowed to regrow in presence or absence (placebo, indicated as control) of the chemical chaperone 4-PBA. In detail, 5 groups of zebrafish were analyzed: WT, *Chi*/+ and *p3h1*$^{-/-}$ controls, *Chi*/+ and *p3h1*$^{-/-}$ 4-PBA treated. After amputation each zebrafish was kept in 200 mL of zebrafish water and half of the volume was replaced every day as already described [17]. In treated zebrafish tanks, 0.05 mM 4-PBA was added daily and its effect evaluated at 3, 5, 7 or 14 dpa depending on the experiment.

Whole-mount immunofluorescence on caudal fins

Amputated caudal fins from WT, *Chi*/+ and *p3h1*$^{-/-}$ were fixed in 4% PFA in PBS o/n at 4 °C and decalcified in 0.5 M EDTA pH 7.4 at 4 °C for four days. Samples were permeabilized in 1% v/v Triton X-100 for 1 hour at RT, rinsed three times in wash solution (0.8% v/v Triton X-100 in PBS) for 5 min at RT and incubated in saturation solution (0.8% v/v Triton X-100, 1% v/v DMSO, 5% BSA in PBS) for 4 h at RT. Samples were then incubated in saturation solution containing primary antibodies o/n at 4 °C under gentle agitation (Supplementary Table 2). As for primary antibodies, samples were incubated in saturation solution containing the secondary antibodies o/n at 4 °C under gentle agitation, quickly rinsed in wash solution at RT and finally incubated with 0.5 μg/ml 4′,6-diamidino-2-phenylindole (DAPI, Sigma-Aldrich) for 10 min. Dako (Agilent) was used for mounting. Images of the 2−3 lateral fin rays (excluding the most-lateral fin ray) were acquired by confocal microscope TCS SP8 (Leica). GFP intensity was measured in each segment and normalized to segment area or width using Fiji (ImageJ). GFP+ cells inside the segments were counted using the Cell counter tool on Fiji (ImageJ) and normalized to segment area. Intensity measurements along fin rays were done with the Plot profile tool in Fiji (ImageJ).

Immunofluorescence on sections

Amputated caudal fins from WT, *Chi*/+ and *p3h1*$^{-/-}$ were fixed in 4% PFA in PBS o/n at 4 °C. Samples were embedded in 1.5% w/v agarose/5% w/v sucrose in PBS and agarose blocks were kept in 30% sucrose in PBS o/n at 4 °C. Agarose blocks were then immersed in optimum cutting temperature compound (OCT, Histoline) and snap frozen in dry ice. Frozen blocks were stored at −80 °C until cryosectioning. Thick sections (16 μm) were obtained using a Leica CM1850 UV cryostat at −22 °C.

Cryosections were incubated 30 min in saturation buffer (1% BSA in PBS) at RT. Primary antibodies were diluted in saturation buffer and applied on sections for 1 hour at RT (Supplementary Table 2). Sections were then rinsed four times, 5 min each, in PBS at RT. Secondary antibodies were diluted in saturation buffer and applied on sections for 1 hour at RT. Sections were rinsed and then incubated in PBS containing Hoechst or DAPI 1:4000 for 5 min at RT. Finally, sections were rinsed in PBS and then in ddH_2O, mounted with Dako (Agilent), and stored in the dark at 4 °C until imaging.

Oil Red O staining

Oil Red O staining was performed on cryosections. For the staining, sections were let air dry for at least 30 min and then fixed in 10% neutral buffered formalin (Sigma-Aldrich). Slides were quickly dipped in 60% isopropanol and stained in 0.18% Oil Red O solution. After washing with 60% isopropanol and water, samples were counterstained with Mayer's Hematoxylin (Sigma-Aldrich) and mounted with Mowiol. Images were acquired using a Leica DM6B wide-field microscope equipped with a DFC7000T camera.

For quantification, an area of $\sim 3 \times 10^3$ μm^2, traced starting 50 μm far from the distal point of the caudal fin, was measured on 63X images. The number of lipid drops was then counted inside the area using the Cell counter tool on Fiji (Image J) software.

Transmission electron microscopy (TEM)

Following anesthesia, caudal fin biopsies were obtained from adult WT and *Chi*/+ zebrafish and rapidly transferred in Karnowsky fixative (0.1 M sodium cacodylate, pH 7.8, 1.5% v/v glutaraldehyde, 4% w/v paraformaldehyde) overnight at 4 °C. Samples were then decalcified in 14% w/v EDTA pH

7.1 at 4 °C, for 24 h for *Chi*/+ and 48 h for WT. The samples were then post-fixed in 2% w/v OsO_4 in H_2O for 2 h at RT, rinsed in distilled water and dehydrated in ethanol. The specimens were infiltrated with LR White acrylic resin overnight at 4 °C and polymerized in gelatin capsules at 60 °C for 24 h. Thick sections (60−70 nm) were cut on a Reichert OM-U3 ultramicrotome with a diamond blade and collected on 300-mesh nickel grids. The grids were finally stained with saturated aqueous uranyl acetate followed by lead citrate and observed with a Zeiss EM900 electron microscope, operated at 80 kV with an objective aperture of 30 mm.

Swimming behavior analysis

Swimming behavior of 10 mpf *Chi*/+ and WT zebrafish (n = 8 for each genotype) was analyzed in a custom-made dark observation chamber (Noldus) equipped with the Basler GenICam capturing 25 frames/second for top-view image acquisition. Data was analyzed using the EthoVision XT 17 software (Noldus). Zebrafish were placed individually in a tank (16 cm (L) x 10 cm (W) x 8 cm (H)) and were allowed to acclimatize for 10 min prior to a 10-minute analysis period. The complete experiment was performed in the dark. For each zebrafish, nose-point, center-point and tail-base detection was performed in the EthoVision software. Movement was expressed as total distance travelled (in cm) during the 10 min analysis period. To obtain information about the difference in tail movement, the ratio of the total distance moved by the tail-base over the center-point was calculated and is coined the tail/center movement ratio. The swimming pattern was analyzed in the Ethovision software using the Track Visualization module displaying the movement of the center-point in red and the tail-base in purple. Representative profiles where the animals were moving a straight path were selected for publication to illustrate the tail movement. Absolute head direction meandering was calculated automatically by dividing the turn angle by the distance moved in the EthoVision software and is a measure to compare turning in animals that move at different speeds.

Statistical analysis

All values are expressed as mean ± standard deviation (SD) except when indicated. Statistical analysis of data was performed with GraphPad Prism 9.3.1. Student's t test was used for unpaired data applying Welsh's correction when samples had significantly different SDs. Multiple comparisons were conducted using ordinary one-way ANOVA with Dunnett's post hoc test or two-way ANOVA with Tukey's post hoc test. Normality was tested through the Shapiro-Wilk's test. A $P < 0.05$ was considered significant.

Declaration of Competing Interest

The authors report no conflict of interest.

Acknowledgments

We thank the OPBA of the University of Pavia for supporting in animal protocol drawing up. We thank the animal facility "Centro di servizio per la gestione unificata delle attività di stabulazione e di radiobiologia" of the University of Pavia, Pavia, Italy, for animal care. We thank Alice Giusto for help with experiments. We acknowledge Dr. Patrizia Vaghi and Dr. Amanda Oldani, Centro Grandi Strumenti, University of Pavia, Italy, for providing confocal and widefield microscopy support. We are grateful to Dr. Anna Jaźwińska for her useful comments on immunofluorescence experiments.

Author's contributions

Conceptualization: V.D., F.T., A.F.; Methodology: V.D., F.T., C. M., D.S., M.B.; Validation: V.D., D.S.; Formal analysis: V.D., F.T., D.S.; Resources: M.B., A.W., P. J. C., F.R., A.F.; Data curation: V.D., F.T., D.S., A.W., A.F.; Writing - original draft: V.D., A.F.; Writing - review & editing: all the coauthors; Supervision: A.F.; Project administration: A.F.; Funding acquisition: D.S., A.F.

Funding

This research was funded by a Grant of the Italian Ministry of Education, University and Research (MIUR) to the Department of Molecular Medicine of the University of Pavia under the initiative "Dipartimenti di Eccellenza (2018−2022 and 2023-2027)" and by the support of Associazione Italiana Osteogenesi Imperfetta (ASITOI) to AF. DS is a senior postdoctoral researcher (12Q5920N) supported by the Research Foundation Flanders. The funders had no role in study design, data collection and analysis, decision to publish, or preparation of the manuscript.

Supplementary materials

Supplementary material associated with this article can be found in the online version at doi:10.1016/j.matbio.2023.06.003.

Received 23 March 2023;
Received in revised form 25 May 2023;
Accepted 16 June 2023
Available online 17 June 2023

Keywords:
Cell differentiation;
Collagen;
Fin regeneration;
Osteogenesis imperfecta;
Zebrafish

References

[1] M. Jovanovic, G. Guterman-Ram, J.C. Marini, Osteogenesis Imperfecta: mechanisms and Signaling Pathways Connecting Classical and Rare OI Types, Endocr. Rev. 43 (1) (2022) 61–90.
[2] D.O. Sillence, A. Senn, D.M. Danks, Genetic heterogeneity in osteogenesis imperfecta, J. Med. Genet. 16 (2) (1979) 101–116.
[3] J.C. Marini, A. Forlino, H.P. Bächinger, N.J. Bishop, P.H. Byers, A. Paepe, et al., Osteogenesis imperfecta, Nat. Rev. Dis. Primers 3 (2017) 17052.
[4] Y. Ishikawa, H.P. Bächinger, A molecular ensemble in the rER for procollagen maturation, Biochim. Biophys. Acta 1833 (11) (2013) 2479–2491.
[5] D.M. Hudson, D.R. Eyre, Collagen prolyl 3-hydroxylation: a major role for a minor post-translational modification? Connect. Tissue Res. 54 (4−5) (2013) 245–251.
[6] R. Besio, N. Garibaldi, L. Leoni, L. Cipolla, S. Sabbioneda, M. Biggiogera, et al., Cellular stress due to impairment of collagen prolyl hydroxylation complex is rescued by the chaperone 4-phenylbutyrate, Dis. Model. Mech. 12 (6) (2019).
[7] F. Tonelli, S. Cotti, L. Leoni, R. Besio, R. Gioia, L. Marchese, et al., Crtap and p3h1 knock out zebrafish support defective collagen chaperoning as the cause of their osteogenesis imperfecta phenotype, Matrix Biol. 90 (2020) 40–60.
[8] R. Gioia, C. Panaroni, R. Besio, G. Palladini, G. Merlini, V. Giansanti, et al., Impaired osteoblastogenesis in a murine model of dominant osteogenesis imperfecta: a new target for osteogenesis imperfecta pharmacological therapy, Stem Cell. 30 (7) (2012) 1465–1476.
[9] L.S. Mirigian, E. Makareeva, E.L. Mertz, S. Omari, A.M. Roberts-Pilgrim, A.K. Oestreich, et al., Osteoblast malfunction caused by cell stress response to procollagen misfolding in α2(I)-G610C mouse model of osteogenesis imperfecta, J. Bone Miner. Res. 31 (8) (2016) 1608–1616.
[10] H. Li, X. Jiang, J. Delaney, T. Franceschetti, I. Bilic-Curcic, J. Kalinovsky, et al., Immature osteoblast lineage cells increase osteoclastogenesis in osteogenesis imperfecta murine, Am. J. Pathol. 176 (5) (2010) 2405–2413.
[11] K. Howe, M.D. Clark, C.F. Torroja, J. Torrance, C. Berthelot, M. Muffato, et al., The zebrafish reference genome sequence and its relationship to the human genome, Nature 496 (7446) (2013) 498–503.
[12] F. Tonelli, J.W. Bek, R. Besio, A. De Clercq, L. Leoni, P. Salmon, et al., Zebrafish: a resourceful vertebrate model to investigate skeletal disorders, Front. Endocrinol. (Lausanne) 11 (2020) 489.
[13] K. Henke, J.M. Daane, M.B. Hawkins, C.M. Dooley, E.M. Busch-Nentwich, D.L. Stemple, et al., Genetic screen for postembryonic development in the Zebrafish (Danio rerio): dominant mutations affecting adult form, Genetics 207 (2) (2017) 609–623.
[14] C. Gistelinck, R.Y. Kwon, F. Malfait, S. Symoens, M.P. Harris, K. Henke, et al., Zebrafish type I collagen mutants faithfully recapitulate human type I collagenopathies, Proc. Natl. Acad. Sci. U. S. A. 115 (34) (2018) E8037-E46.
[15] E. Kague, P. Roy, G. Asselin, G. Hu, J. Simonet, A. Stanley, et al., Osterix/Sp7 limits cranial bone initiation sites and is required for formation of sutures, Dev. Biol. 413 (2) (2016) 160–172.
[16] S. Fisher, P. Jagadeeswaran, M.E. Halpern, Radiographic analysis of zebrafish skeletal defects, Dev. Biol. 264 (1) (2003) 64–76.
[17] R. Gioia, F. Tonelli, I. Ceppi, M. Biggiogera, S. Leikin, S. Fisher, et al., The chaperone activity of 4PBA ameliorates the skeletal phenotype of Chihuahua, a zebrafish model for dominant osteogenesis imperfecta, Hum. Mol. Genet. 26 (15) (2017) 2897–2911.
[18] M. Gemberling, T.J. Bailey, D.R. Hyde, K.D. Poss, The zebrafish as a model for complex tissue regeneration, Trend. Genet. 29 (11) (2013) 611–620.
[19] F. Knopf, C. Hammond, A. Chekuru, T. Kurth, S. Hans, C.W. Weber, et al., Bone regenerates via dedifferentiation of osteoblasts in the zebrafish fin, Dev. Cell 20 (5) (2011) 713–724.
[20] S. Sousa, N. Afonso, A. Bensimon-Brito, M. Fonseca, M. Simões, J. Leon, et al., Differentiated skeletal cells contribute to blastema formation during zebrafish fin regeneration, Development 138 (18) (2011) 3897–3905.
[21] N. Blum, G. Begemann, Osteoblast de- and redifferentiation are controlled by a dynamic response to retinoic acid during zebrafish fin regeneration, Development 142 (17) (2015) 2894–2903.
[22] F. Tonelli, L. Leoni, V. Daponte, R. Gioia, S. Cotti, I.A.K. Fiedler, et al., Zebrafish Tric-b is required for skeletal development and bone cells differentiation, Front. Endocrinol. (Lausanne) 14 (2023) 1002914.
[23] C. Pfefferli, A. Jaźwińska, The art of fin regeneration in zebrafish, Regeneration (Oxf) 2 (2) (2015) 72–83.
[24] J. Cardeira, P.J. Gavaia, I. Fernández, I.F. Cengiz, J. Moreira-Silva, J.M. Oliveira, et al., Quantitative assessment of the regenerative and mineralogenic performances of the zebrafish caudal fin, Sci. Rep. 6 (2016) 39191.
[25] M.T. Valenti, G. Marchetto, M. Mottes, L. Dalle Carbonare, Zebrafish: a suitable tool for the study of cell signaling in bone, Cells. 9 (8) (2020).
[26] I.M. Sehring, G. Weidinger, Recent advancements in understanding fin regeneration in zebrafish, Wiley Interdiscip. Rev. Dev. Biol. 9 (1) (2020) e367.
[27] T. van der Meulen, S. Kranenbarg, H. Schipper, J. Samallo, J.L. van Leeuwen, H. Franssen, Identification and characterisation of two runx2 homologues in zebrafish with different expression patterns, Biochim. Biophys. Acta 1729 (2) (2005) 105–117.
[28] A. Smith, F. Avaron, D. Guay, B.K. Padhi, M.A. Akimenko, Inhibition of BMP signaling during zebrafish fin regeneration disrupts fin growth and scleroblasts differentiation and function, Dev. Biol. 299 (2) (2006) 438–454.
[29] D. Imrie, K.C. Sadler, White adipose tissue development in zebrafish is regulated by both developmental time and fish size, Dev. Dyn. 239 (11) (2010) 3013–3023.

[30] P.E. Witten, A. Huysseune, A comparative view on mechanisms and functions of skeletal remodelling in teleost fish, with special emphasis on osteoclasts and their function, Biol. Rev. Camb. Philos. Soc. 84 (2) (2009) 315–346.
[31] J. Cardeira-da-Silva, A. Bensimon-Brito, M. Tarasco, A.S. Brandão, J.T. Rosa, J. Borbinha, et al., Fin ray branching is defined by TRAP+ osteolytic tubules in zebrafish, Proc. Natl. Acad. Sci. U. S. A. 119 (48) (2022) e2209231119.
[32] H.L. Ansorge, X. Meng, G. Zhang, G. Veit, M. Sun, J.F. Klement, et al., Type XIV Collagen regulates fibrillogenesis: premature Collagen Fibril growth and tissue dysfunction in null mice, J. Biol. Chem. 284 (13) (2009) 8427–8438.
[33] Y. Izu, S.M. Adams, B.K. Connizzo, D.P. Beason, L.J. Soslowsky, M. Koch, et al., Collagen XII mediated cellular and extracellular mechanisms regulate establishment of tendon structure and function, Matrix Biol. 95 (2021) 52–67.
[34] A. Forlino, J.C. Marini, Osteogenesis imperfecta, Lancet 387 (10028) (2016) 1657–1671.
[35] M. Jain, A. Tam, J.R. Shapiro, R.D. Steiner, P.A. Smith, M.B. Bober, et al., Growth characteristics in individuals with osteogenesis imperfecta in North America: results from a multicenter study, Genet. Med. 21 (2) (2019) 275–283.
[36] N. Fratzl-Zelman, A.M. Barnes, M. Weis, E. Carter, T.E. Hefferan, G. Perino, et al., Non-Lethal Type VIII Osteogenesis Imperfecta Has Elevated Bone Matrix Mineralization, J. Clin. Endocrinol. Metab. 101 (9) (2016) 3516–3525.
[37] J.A. Vranka, E. Pokidysheva, L. Hayashi, K. Zientek, K. Mizuno, Y. Ishikawa, et al., Prolyl 3-hydroxylase 1 null mice display abnormalities in fibrillar collagen-rich tissues such as tendons, skin, and bones, J. Biol. Chem. 285 (22) (2010) 17253–17262.
[38] K.D. Poss, M.T. Keating, A Nechiporuk, Tales of regeneration in zebrafish, Dev. Dyn. 226 (2) (2003) 202–210.
[39] F. Rauch, R. Travers, A.M. Parfitt, F.H. Glorieux, Static and dynamic bone histomorphometry in children with osteogenesis imperfecta, Bone 26 (6) (2000) 581–589.
[40] C.M. Kaneto, P.S. Pereira Lima, K.L. Prata, J.L. Dos Santos, J.M. de Pina Neto, R.A. Panepucci, et al., Gene expression profiling of bone marrow mesenchymal stem cells from Osteogenesis Imperfecta patients during osteoblast differentiation, Eur. J. Med. Genet. 60 (6) (2017) 326–334.
[41] T.E. Uveges, P. Collin-Osdoby, W.A. Cabral, F. Ledgard, L. Goldberg, C. Bergwitz, et al., Cellular mechanism of decreased bone in Brtl mouse model of OI: imbalance of decreased osteoblast function and increased osteoclasts and their precursors, J. Bone Miner. Res. 23 (12) (2008) 1983–1994.
[42] N. Fratzl-Zelman, H.P. Bächinger, J.A. Vranka, P. Roschger, K. Klaushofer, F. Rauch, Bone matrix hypermineralization in prolyl-3 hydroxylase 1 deficient mice, Bone 85 (2016) 15–22.
[43] R. Morello, T.K. Bertin, Y. Chen, J. Hicks, L. Tonachini, M. Monticone, et al., CRTAP is required for prolyl 3- hydroxylation and mutations cause recessive osteogenesis imperfecta, Cell 127 (2) (2006) 291–304.
[44] G.L. Semenza, HIF-1 and mechanisms of hypoxia sensing, Curr. Opin. Cell Biol. 13 (2) (2001) 167–171.
[45] A.J. Leger, A. Altobelli, L.M. Mosquea, A.J. Belanger, A. Song, S.H. Cheng, et al., Inhibition of osteoclastogenesis by prolyl hydroxylase inhibitor dimethyloxallyl glycine, J. Bone Miner. Metab. 28 (5) (2010) 510–519.
[46] P.A. Hulley, T. Bishop, A. Vernet, J.E. Schneider, J.R. Edwards, N.A. Athanasou, et al., Hypoxia-inducible factor 1-alpha does not regulate osteoclastogenesis but enhances bone resorption activity via prolyl-4-hydroxylase 2, J. Pathol. 242 (3) (2017) 322–333.
[47] A. Gagliardi, R. Besio, C. Carnemolla, C. Landi, A. Armini, M. Aglan, et al., Cytoskeleton and nuclear lamina affection in recessive osteogenesis imperfecta: a functional proteomics perspective, J. Proteom. 167 (2017) 46–59.
[48] C. Gerri, R. Marín-Juez, M. Marass, A. Marks, H.M. Maischein, D.Y.R. Stainier, Hif-1α regulates macrophage-endothelial interactions during blood vessel development in zebrafish, Nat. Commun. 8 (2017) 15492.
[49] P. Castagnola, S. Tavella, D.R. Gerecke, B. Dublet, M.K. Gordon, J. Seyer, et al., Tissue-specific expression of type XIV collagen–a member of the FACIT class of collagens, Eur. J. Cell Biol. 59 (2) (1992) 340–347.
[50] H.L. Bader, E. Lambert, A. Guiraud, M. Malbouyres, W. Driever, M. Koch, et al., Zebrafish collagen XIV is transiently expressed in epithelia and is required for proper function of certain basement membranes, J. Biol. Chem. 288 (10) (2013) 6777–6787.
[51] P. Nauroy, A. Guiraud, J. Chlasta, M. Malbouyres, B. Gillet, S. Hughes, et al., Gene profile of zebrafish fin regeneration offers clues to kinetics, organization and biomechanics of basement membrane, Matrix Biol. (2019) 82–101 75-76.
[52] T. Kato, K. Nakayasu, A. Kanai, T. Nishiyama, Y. Imamura, T. Hayashi, Distribution and isoform characterization of type XII collagen in bovine cornea, Ophthalmic Res. 32 (5) (2000) 215–221.
[53] H.L. Bader, D.R. Keene, B. Charvet, G. Veit, W. Driever, M. Koch, et al., Zebrafish collagen XII is present in embryonic connective tissue sheaths (fascia) and basement membranes, Matrix Biol. 28 (1) (2009) 32–43.
[54] C. Panaroni, R. Gioia, A. Lupi, R. Besio, S.A. Goldstein, J. Kreider, et al., In utero transplantation of adult bone marrow decreases perinatal lethality and rescues the bone phenotype in the knockin murine model for classical, dominant osteogenesis imperfecta, Blood 114 (2) (2009) 459–468.
[55] A. Reich, W. Cabral, J. Marini, Homogeneous Mutant Collagen in Osteogenesis Imperfecta Model Mice Leads to Improved Bone Phenotype through Multiple Pathways [Abstract P38], Program of the American Society for Bone and Mineral Research Topical Meeting on Bone and Skeletal Muscle Interactions, Kansas City, MO, 2012.
[56] T. Desvignes, A. Carey, J.H. Postlethwait, Evolution of caudal fin ray development and caudal fin hypural diastema complex in spotted gar, teleosts, and other neopterygian fishes, Dev. Dyn. 247 (6) (2018) 832–853.
[57] P.E. Witten, A. Huysseune, B.K Hall, A practical approach for the identification of the many cartilaginous tissues in teleost fish, J. Appl. Ichthyol. 26 (2010) 257–262.
[58] A. Bensimon-Brito, M.L. Cancela, A. Huysseune, P.E. Witten, Vestiges, rudiments and fusion events: the zebrafish caudal fin endoskeleton in an evo-devo perspective, Evol. Dev. 14 (1) (2012) 116–127.
[59] C.C. Huang, T.C. Wang, B.H. Lin, Y.W. Wang, S.L. Johnson, J. Yu, Collagen IX is required for the integrity of collagen II fibrils and the regulation of vascular plexus formation in zebrafish caudal fins, Dev. Biol. 332 (2) (2009) 360–370.
[60] I. Durán, M. Marí-Beffa, J.A. Santamaría, J. Becerra, L. Santos-Ruiz, Actinotrichia collagens and their role in fin formation, Dev. Biol. 354 (1) (2011) 160–172.
[61] J.A. Santamaría, J. Becerra, Tail fin regeneration in teleosts: cell-extracellular matrix interaction in blastemal differentiation, J. Anat. 176 (1991) 9–21.

[62] P. Marzin, V. Cormier-Daire, New perspectives on the treatment of skeletal dysplasia, Ther. Adv. Endocrinol. Metab. 11 (2020) 2042018820904016.
[63] L.A. Mullan, E.J. Mularczyk, L.H. Kung, M. Forouhan, J.M. Wragg, R. Goodacre, et al., Increased intracellular proteolysis reduces disease severity in an ER stress-associated dwarfism, J. Clin. Invest. 127 (10) (2017) 3861–3865.
[64] C. Paganini, C. Gramegna Tota, L. Monti, I. Monti, A. Maurizi, M. Capulli, et al., Improvement of the skeletal phenotype in a mouse model of diastrophic dysplasia after postnatal treatment with N-acetylcysteine, Biochem. Pharmacol. 185 (2021) 114452.
[65] R. Besio, G. Iula, N. Garibaldi, L. Cipolla, S. Sabbioneda, M. Biggiogera, et al., 4-PBA ameliorates cellular homeostasis in fibroblasts from osteogenesis imperfecta patients by enhancing autophagy and stimulating protein secretion, Biochim. Biophys. Acta Mol. Basis Dis. 1864 (2018) 1642–1652 5 Pt A.
[66] N. Garibaldi, B.M. Contento, G. Babini, J. Morini, S. Siciliani, M. Biggiogera, et al., Targeting cellular stress *in vitro* improves osteoblast homeostasis, matrix collagen content and mineralization in two murine models of osteogenesis imperfecta, Matrix Biol. 98 (2021) 1–20.
[67] X. Shi, L. Gong, Y. Liu, K. Hou, Y. Fan, C. Li, et al., 4-phenylbutyric acid promotes migration of gastric cancer cells by histone deacetylase inhibition-mediated IL-8 upregulation, Epigenetics 15 (6–7) (2020) 632–645.
[68] M.J. Tomecka, L.P. Ethiraj, L.M. Sánchez, H.H. Roehl, T.J. Carney, Clinical pathologies of bone fracture modelled in zebrafish, Dis. Model. Mech. 12 (9) (2019).
[69] L.M. McGowan, E. Kague, A. Vorster, E. Newham, S. Cross, C.L. Hammond, Wnt16 elicits a protective effect against fractures and supports bone repair in zebrafish, JBMR Plus 5 (3) (2021) e10461.
[70] J. Vanoevelen, A. Janssens, L.F. Huitema, C.L. Hammond, J.R. Metz, G. Flik, et al., Trpv5/6 is vital for epithelial calcium uptake and bone formation, FASEB J. 25 (9) (2011) 3197–3207.
[71] K.M. Spoorendonk, J. Peterson-Maduro, J. Renn, T. Trowe, S. Kranenbarg, C. Winkler, et al., Retinoic acid and Cyp26b1 are critical regulators of osteogenesis in the axial skeleton, Development 135 (22) (2008) 3765–3774.
[72] S. Vanhauwaert, G. Van Peer, A. Rihani, E. Janssens, P. Rondou, S. Lefever, et al., Expressed repeat elements improve RT-qPCR normalization across a wide range of zebrafish gene expression studies, PLoS One 9 (10) (2014) e109091.